Decreasing Matrix Effect in PGAA

Ph.D. dissertation

by

Péter Pál Ember

Budapest University of Technology and Economics

and

Institute of Isotope and Surface Chemistry,

Chemical Research Centre

Hungarian Academy of Sciences

Budapest. 2003

Nyilatkozat

Alulírott Ember Péter Pál kijelentem, hogy ezt a doktori értekezést magma készítettem, és abban csak a megadott forrásokat használtam fel. Minden olyan részt, amelyet szó szerint vagy azonos tartalommal, de átfogalmazva más forrásból átvettem egyértelműen, a forrás megadásával megjelöltem.

……

TABLE OF CONTENTS

1. Preface

Instead of scientific knowledge, this first chapter contains my thoughts, subjective opinion, and everything that does not fit anywhere else in this work.

In 1998, when I decided to choose a PhD topic about being a "*creator"* of a new kind of measurement device, instead of being a "*user"* and measuring with an existing one, I considered it a big challenge. Now I believe it was definitely more! I expected to publish papers later than "*user"* type PhD students, but did not expect it to take more than three years till the first one. As all instrument inventors our team had to deal with those annoying noise problems. It took more than a year to hunt ground loops, and broken connections to be able to obtain acceptable measurement results. Then – when we were ready to make real measurements – the reactor was stopped because of the installation of the cold neutron source.

At certain phases of the work, I felt it a Sisyphean task, and I was thinking on giving it up, and choosing another topic, more likely some light weight one, with no exciting amplifiers and ground loops, just theorems, papers and pencils.

And here is some pre-acknowledgements: I owe particular thank those who helped me through these desperate times: Fortune, colleagues and friends.

About the first: It might be strange to thank my luck, but I believe science sometimes requires an enormous boost of luck. And I had both explicit and implicit luck. By explicit luck I mean the finding of the solution of a problem by accident, and by implicit luck I mean having just those people around me.

The work described here is not complete. Actually, I believe that a work can not be completed, just stopped at a satisfactory status. New ideas and possibilities emerge every day. I have no desire to finish this work at this state, I will continue to work on it. But it is now at a state complete enough to make my thesis. So please treat his thesis as a snapshot: I got this far.

Péter Pál Ember

2. Introduction

In Prompt Gamma Activation Analysis (PGAA) a frequent problem is the presence of a few strong γ rays emitted by the main ingredients of the sample masking the lower energy transitions of trace elements with their Compton continuum. This is called matrix effect.

The increased selectivity of the coincidence method is expected to decrease the matrix effect. My primary goal was to find cases that are problematic with the traditional PGAA: when the sensitivity of the Compton suppression detection technique decreases because of the matrix effect. and apply the γ-γ coincidence method in those cases. I plan to use two high purity Germanium (HPGe) detectors. No PGAA coincidence measurement with two HPGe can be found in the literature. I planned to create a γ-γ coincidence PGAA setup, and the software required for its proper usage. I planned to determine if the new setup is applicable for analytical purposes, and to find special cases where it can compete with the existing traditional method. I expected that, the closer geometry of the γ-γ coincidence method can balance the lower efficiency of coincidence.

The structure of this work follows the traditional structure of a coursebook:

After this introduction it starts with an overview (Chapter 3) containing the literature summary focusing on subfields which are important for understanding the following sections.

Then the PGAA (prompt gamma activation analysis) experimental station is detailed in chapter 4. This chapter also contains the description of the PGAA-NIPS facility, and the Compton suppressed spectrometer at the Budapest research reactor, and an industrial PGAA application to demonstrate the matrix effect.

Chapter 5 contains my work in a logical order: the description of the NIPS facility and the process of the peak - peak coincidence, the data processing software and the measurements. Some of the measurements were made before the NIPS facility was constructed. At these measurements I marked the information obtained from these measurements, which proved to be important aspect of the planning. It gives some sensation about the procession of the work. An important achievement of my work is the principle of the regional coincidence is put into the middle of the list of measurements. Chapter 6 summarizes my work, and Chapter 7 contains my thesis.

Chapter 8 is a short section about how I plan to continue this work. The acknowledgement and the references sections finalize the work. At the end there are the appendices collecting the parameters of the facilities, and the isotopes used in this work.

3. Literature

3.1. The neutron

Neutrons were discovered by Chadwick in 1932. Since that, many parameters of this particle have been measured with different techniques. Also, countless possible uses have been discovered for numerous fields from radiography to cancer therapy

For the radiation neutron capture measurements introduced in latter sections, the most important parameters of neutron beams are energy and flux. Various different neutron gas energy classifications are known in the literature according to the field that applies the neutrons. The simplest classification of neutron gas by energy is: “fast” and “slow” neutrons. The dividing energy is about 0.5 eV (the cadmium cutoff energy). Another classification is made according to the resonance energies of moderator materials in nuclear reactors: fast neutrons (E>1 MeV), intermediate energy neutrons (1MeV>E>1eV) and slow neutrons (E<1eV). Table 1 shows a third, more complex classification for neutron beams.

Table 1 Classification of neutron gas or beam by energy

Fast	>100 eV
Epithermal	100 eV – 0.025 eV
Thermal	**≈ 0.02525 eV**
Cold	0.025 eV – 10^{-5} eV
Very cold	10^{-5} eV – 10^{-7} eV
Ultra cold	< 10^{-7} eV

Thermal neutron gas is neutron gas characterized by Maxwellian energy distribution of room temperature (T=293 K). Their main energy is $E_T=kT$. The corresponding average velocity is 2198 m/s, calculated from the energy with the $½mv^2$ equation. The corresponding mean wavelength is 1,797 Å, calculated from the $E=h^2/2m\lambda^2$ equation.

The neutron flux definition of a neutron gas is:

$$\phi(\underline{r},\underline{v},t) = v \cdot N(\underline{r},\underline{v},t) \qquad \left[\frac{neutron}{cm^2 \cdot s}\right]$$

Where $\underline{v}$ is the velocity of the neutrons [cm/s], $N(\underline{r},\underline{v},t)$ is the neutron density at a given $\underline{r}$ position at a given t time [1/cm^3]

In the cases of parallel neutron beam techniques this product is the number of neutrons hitting a 1 cm^2 surface perpendicular to the direction of the beam every second.

3.1.1. Interactions of neutrons with matter

If a charged particle (like proton, deuteron or α particle) interacts with a nucleus, it must carry sufficient energy to penetrate the Coulomb barrier of that nucleus. Neutrons have no charge and therefore can penetrate any nucleus without interacting with its Coulomb field. The neutron-matter interaction can be denoted as follows:

$$n+T \rightarrow K^* \rightarrow X+Y \qquad \text{or} \qquad T(n,Y)X$$

It represents the 3 states of the reaction. The left side represents the initial state, when neutron *n* approaches the nuclei *T*, but is still out of the range of the nuclear forces. In the middle there is an intermediate state, and the right side represents the final state, when reaction products X and Y leave the range of the nuclear forces.

The possible reactions are elastic scattering (n,n), inelastic scattering (n,n'), radiating capture (n,γ), charged particle (n,p), (n,d), (n,α) reactions, neutron emission (n, xn) and fission (n,f). For the present work, the most important reaction is the (n, γ) reaction. In this case the K* intermediate nucleus captures the neutron, and the outgoing gamma photons carry away the excitation energy. This reaction can take place at any neutron energy.

The energy and intensity of the emitted gamma photons is characteristic of the nucleus, so the nucleus can be identified by its emitted gamma photons. This is the main concept underlying the neutron activation analysis methods described in later sections.

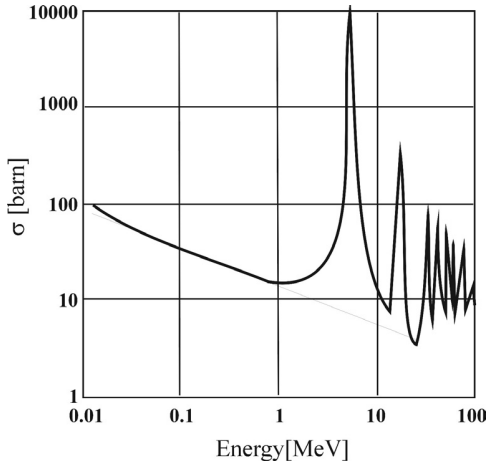

Figure 1 Ag(n,γ) reaction cross section as the function of the neutron energy

The probability of a certain reaction with a certain nucleus can be characterized by its cross section σ. The unit of cross section is: *1 barn* $=10^{-28}$ m^2. The cross section of neutron interactions changes dramatically with the neutron energy. For the energy range used for PGAA (thermal or lower neutron energy) this energy function of the radiative capture reaction is extremely simple: for most elements it is proportional to the reciprocal of the *v* velocity of

the neutron. This is the so called 1/v law. At certain energies, the radiative capture cross section is extremely high. These are the so called resonance peaks. Figure 1 shows an example for the 1/v law and the resonance peaks.

In the case of collimated neutron beams the number of reactions caused by a neutron beam in a given irradiated target (reaction rate) can be calculated by multiplying the neutron flux of the beam by the cross section of the irradiated material:

$$\_F(\underline{r},\underline{v},t)=\sigma\cdot\phi(\underline{r},\underline{v},t)$$

The isotopes listed in Table 2 have a thermal neutron capture cross section high enough to serve as shielding against neutrons.

Table 2 Neutron capture cross-sections of some isotopes [Firestone 96]

^{3}He	(n_{th}, p)	5333 barns	^{6}Li	(n_{th}, α)	940 barns
^{10}B	(n_{th}, α)	3837 barns	^{113}Cd	(n_{th}, γ)	20600 barns
^{149}Sm	(n_{th}, γ)	40140 barns	^{155}Gd	(n_{th}, γ)	60900 barns
^{235}U	(n_{th}, f)	582 barns	^{157}Gd	(n_{th}, γ)	254000 barns

Except for ^{3}He and ^{6}Li, the neutron reaction of the listed elements produces gamma radiation. Thus ^{6}Li loaded materials can be used as neutron protection even close to gamma sensitive detectors. Although boron produces gammas, but has a bigger cross section, so it can be used at places further from the detectors. The neutron reactions of ^{6}Li and ^{10}B are as follows [Beckurts 64]:

$$^{6}_{3}\mathrm{Li}+^{1}_{0}\mathrm{n}\rightarrow{}^{3}_{1}\mathrm{H}+^{4}_{2}\mathrm{He}+4{,}786\ \mathrm{MeV}$$

$$^{10}_{5}\mathrm{B}+^{1}_{0}\mathrm{n}\rightarrow{}^{7}_{3}\mathrm{Li}+^{4}_{2}\mathrm{He}+\begin{cases}2{,}79\ \mathrm{MeV}\ \ (6{,}1\,\%)\\ 2{,}31\ \mathrm{MeV}\ \ (93{,}9\,\%)+0{,}478\mathrm{MeV}\gamma\end{cases}$$

Neutron scattering also has a very important aspect called total external reflection:

Most materials have a neutronoptical index of reflection less than 1, so neutrons in vacuum (or air) can be totally reflected from the vacuum-matter border if the glancing angle is smaller than a critical angle:

$$\theta_C=\lambda\cdot\sqrt{\frac{Na}{\pi}}=\lambda\cdot\gamma_C$$

where λ is the neutron wavelength, N is the number of scattering nuclei per unit volume, a is the free scattering length. This phenomenon makes the creation of neutron guides possible. A neutron guide is a totally reflective walled tube which can guide the neutron beams for tens of meters without major losses.

3.2. Laboratory neutron sources

There are five types of artificial neutron sources available for laboratory use:

1. Radioisotope sources

   These sources are based on the (α,n) reaction of appropriate isotopes, such as exothermic reaction $^{9}Be(\alpha,n)^{12}C$ with Q=5.71 MeV. Sources are constructed using a mixture of this element with a compound of an α source like polonium or radium. These sources produce neutrons in the range of 0-13 MeV, and a background γ radiation, which can be a disadvantage.

   The isotope ^{252}Cf has a half life of approximately 2.6 years for spontaneous fission. This isotope is also a useful source of neutrons with an average energy of 2.3MeV.

2. Photoneutron sources

   Only the following two photonuclear reactions have sufficient yield to create a useful neutron source:

   $$^{2}H(\gamma,n)^{1}H \qquad Q=-2.23MeV$$
   $$^{9}Be(\gamma,n)^{8}Be \qquad Q=-1.67MeV$$

   Deuterium oxide or metallic beryllium targets must be exposed to γ-rays from enclosed radioisotopes. The most commonly used isotopes are β emitters: ^{24}Na, ^{72}Ga, ^{124}Sb, ^{140}La. These sources produce neutrons with homogeneous energy distribution.

3. Accelerator sources

   Several possibilities exist for generating neutrons of different energy distribution with various kinds of accelerators.

   One of the simplest techniques is to generate photoneutrons using the bremsstrahlung of an electron accelerator.

4. Spallation sources.

   Nuclear reactions generated by particles with energies of 100 MeV or higher can eject numerous neutrons from the special target. For example 1 GeV protons can produce a neutron yield of ~2 neutron/proton on beryllium, and ~40 on uranium target.

5. Nuclear reactors (fission sources)

Various types of nuclear reactors are very effective and commonly used neutron sources. They are operating on the principle of the controlled and self-sustaining chain-reaction of neutron-induced nuclear fission:

Some heavy nuclei can break into smaller fragments after capturing a neutron. This fission process releases approximately 200 MeV energy carried away by the fission products and accompanying β, γ, neutrino and neutron radiations. The fission can produce enough neutrons to keep the process going by inducing more and more fission reactions. This is called chain reaction.

A system is "*critical*" if the number of neutrons causing a new fission is exactly 1 for each reaction, "*supercritical*" if >1 and "*subcritical*" if <1. A nuclear reactor is a critical, a nuclear bomb is a supercritical system. Figure 2 shows these two cases.

The first nuclear reactor which successfully supported a self-sustaining chain reaction was built in 1942 by Fermi and his associates [Fermi 47].

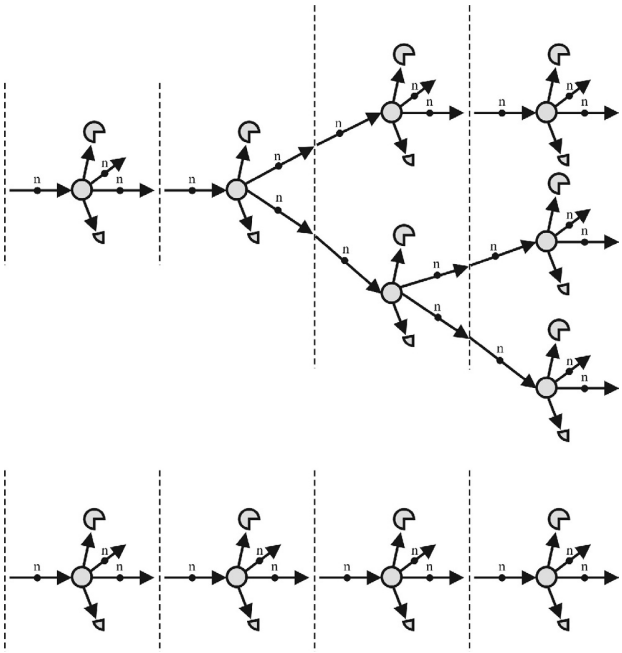

Figure 2 Supercritical (above) and critical (below) systems

Special kinds of reactors are the pulsed reactors that are periodically driven to be supercritical causing very high neutron flux. The safety of such an instrument can be obtained is due to the negative temperature coefficient of the selected reaction or moderator. These reactors are built only for research purposes, to create very high flux of neutron impulses.

3.3. Thermal reactors as neutron sources

Some fissionable nuclei e.g. ^{233}U, ^{235}U or ^{239}Pu undergo fission more likely on low energy neutron (0,01-0,1 eV) bombardment, while the fission reaction of some other e.g. ^{232}Th, ^{238}U and ^{237}Np require neutrons with at least 1 MeV energy. Depending on the energy of neutrons causing the fission, reactors can be classified into thermal, intermediate and fast reactors. More than 99 % of the existing reactors are thermal reactors using ^{235}U fuel.

Thermal neutron induced ^{235}U fission produces an average of 2.43 neutrons. About 99.36% of these neutrons are emitted within a very short period of time ($4 \cdot 10^{-14}$s) after the fission (prompt neutrons). If the fission products still have neutron excess, they can emit additional neutrons with a half life up to 55 s (late neutrons). These late neutrons are important for the controllability of the reactors. Not all neutrons captured by fissionable nuclei cause fission. The probability of a new fission reaction is the ratio of the macroscopic cross sections: $\sigma_{fission} / \sigma_{Total}$. For ^{235}U this ratio is 0.85. So theoretically an average of 2.07 new neutrons can cause a new fission after each capture in ^{235}U. The criticality of the reactor requires 1.0, so the reaction has plenty of reserves.

The prompt neutron energy spectrum can be described with the semi-empiric Watt formula. The formula for ^{235}U fueled thermal reactors is the following:

$$N(E_n) = 0{,}484 \cdot \sinh\sqrt{2E_n}\, e^{-E_n}$$

where E_n is the neutron Energy in MeV. This formula is illustrated in Figure 3.

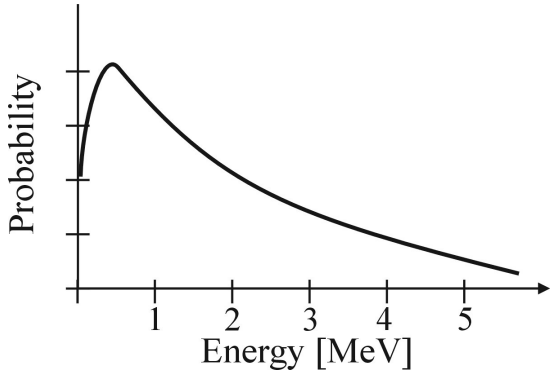

Figure 3 Prompt neutron energy spectrum in a ^{235}U fueled thermal reactor

As can be seen in Figure 3, prompt neutrons have a most probable energy of about 0.7 MeV, and an average energy of 2 MeV (late neutrons have ~10 times lower energy). A portion of the prompt neutrons have energies of several MeV. These fast neutrons must be slowed down in order to increase their chance to cause additional fission. This can be done by scattering the

neutrons on light nuclei. The process is called moderation and is illustrated in Figure 4. The most commonly used moderation materials are hydrogen in the form of H_2O, deuteron in the form of D_2O and carbon as graphite.

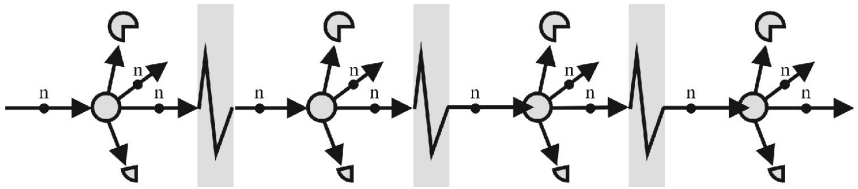

Figure 4 Chain reaction in thermal reactors

In a reactor the fuel and the moderator must be mixed. The most common solution is the usage of fuel rods with hermetic cover in a quadratic or hexagonal lattice. The space between the rods is filled with the moderator material. The area where the fuel rods are positioned (so that the chain reaction can be realized) is called active zone. In practice all real reactor zones are surrounded with reflection material capable of reflecting the neutrons. Figure 5 shows the thermal and fast neutron flux distribution in a reactor with reflector.

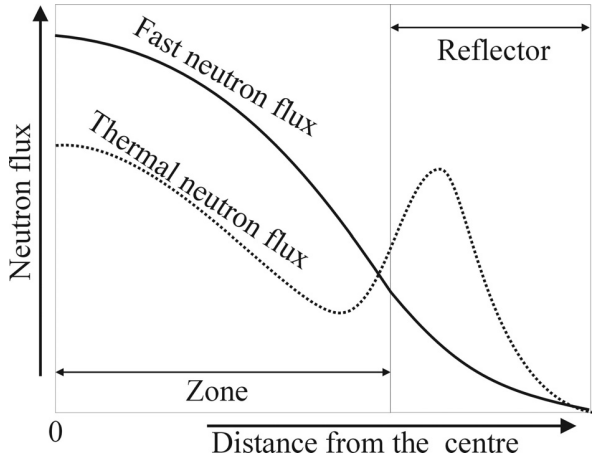

Figure 5 Thermal and fast neutron flux distribution in a reactor with reflector

As shown in the figure, the thermal to fast neutron flux ratio is highest in the reflector. Thus, thermal neutron irradiations can be done in the reflector part, without disturbing the active zone. Also thermal neutron tubes for neutron guides should start from the reflector.

The fission reaction and the decay of the fission products create a very large number of gamma photons in the active zone. This can cause a high gamma background at the end of the neutron guides. By positioning irradiation tubes tangentially, direct view of the zone can be avoided, decreasing gamma background dramatically. Another technique is the use of a

curved guide. The combination of the two can produce a neutron beam suitable for gamma sensitive instruments.

3.4. The prompt gamma activation analysis

Right after the discovery of the neutron, experiments were started to investigate the different reactions between this particle and various materials. In 1934 high energy γ emission was detected when irradiating a hydrogen containing sample with neutrons [Ama 34]. It was the first prompt gamma experiment. The prompt gamma photons are those gamma photons which are emitted almost instantaneously by neutron irradiated material due to (n, γ) reaction.

It was discovered very early that neutron irradiation can create radioactive isotopes. In 1936 Hevesy György started to exploit this phenomenon for the determination of the elemental composition of the irradiated material. This method is called the Neutron Activation Analysis (**NAA**). Due to its accuracy and ease of use, NAA stations can be found at almost all research reactors around the world.

The possibility to use the prompt gamma radiation for the same purpose came with the neutron guide technique in the late sixties. The first prompt gamma activation analysis (**PGAA**) facility was constructed in 1969 in Saclay; Grenoble was second in 1973 [Hen 73]. The method became popular, and now more and more research reactors have neutron guide with PGAA port. The most well-known PGAA instruments in the world [Molnár 98] are operated at KFA Juelich in Germany (23 MW FRJ-2 reactor), NIST in the USA (20 MW NBSR reactor) [Lindstrom 93], JAERI Tokai in Japan (20 MW JRR-3M reactor) [Yonezawa 93], ILL Grenoble in France. Also two new ones are under construction: one in Munich, Germany, and one in Korea.

3.4.1. Principle of the activation analysis method

Figure 6 illustrates the principle of prompt gamma activation analysis. The nucleus $({}^{A}_{Z}X)$ can absorb neutrons *(n)*. The resulting highly excited compound nuclei $({}^{A+1}_{Z}X^{*})$ has a very short life time (usually $<10^{-16}$ s) and decays by emitting a cascade of γ photons. These γ photons are called prompt γ photons and marked with γ_p in Figure 6.

In a number of cases the ${}^{A+1}_{Z}X$ nucleus is radioactive, and β-decays with a longer life time, while emitting more γ photons marked with γ_d in Figure 6. These decays continue till the nucleus reaches its stable state.

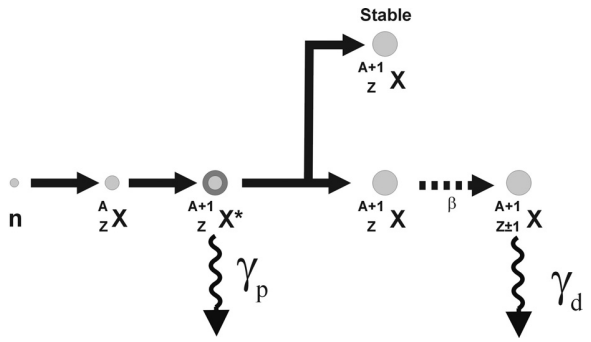

Figure 6 Activation Analysis

Due to the individual level structure of the nuclei, the energy and intensity of the emitted γ_p and γ_d gamma photons are characteristic of the ${}^{A}_{Z}X$ element. If a complex sample is irradiated with a neutron beam, this fingerprint allows the determination of its elemental composition from the measured spectra.

3.4.2. NAA and PGAA

The main difference between prompt gamma activation analysis (PGAA) and the conventional neutron activation analysis (NAA) [Ehmann 91 .Chapter 9.2 pp 271-291] is the stage where gamma photons are detected.

In the case of NAA the sample is irradiated very close to the active zone of the reactor for a given period of time. The measurement takes place in a low background laboratory after some cooling time. This method can detect only the γ_d photons (see Figure 6), so it can not be used if ${}^{A+1}_{Z}X$ is stable or decays too fast. NAA is widely used for trace element detection. For selected elements the sensitivity can be increased by optimizing the irradiation and cooling time.

In the case of PGAA the irradiation and the measurement is simultaneous, so this method can detect both γ_p and γ_d photons. Because of this, PGAA spectra for real samples are much more complex and contain more peaks than the NAA spectra of the same sample.

The most widely used detection instrument for PGAA is a Compton suppressed spectrometer [Belgya, 1996], which greatly reduces the size of the continuum and of the escape peaks. The Compton suppressed spectrometer at the Budapest research reactor is described in Chapter 3.3. Many efforts have been made in various laboratories to improve its analytical sensitivity by reducing the background using well collimated cold-neutron beams. A possible way of further improvement is to change from the traditional Compton suppression detection technique to a more selective one. A natural choice is the use of the γ-γ coincidence technique

with scintillation detectors [Gardner et al., 2000], or with HPGe detectors [Ember et al., 2002]. This latter technique is the subject of this work.

3.4.3. Properties of PGAA

- PGAA transforms only a negligible amount of the sample, thus it is considered nondestructive.
- All elements except helium produce measurable prompt gamma radiation, so PGAA can detect practically all elements of the periodic table.
- Neutrons penetrate the sample deeply, so PGAA provides the average elemental composition of the irradiated volume of the sample.
- PGAA requires minimal sample preparation
- PGAA can produce instant results, and its precision increases with time.
- The detection limit depends on the neutron capture cross section of the target element and the elemental composition of the sample. In several cases, even concentrations under 1 ppm can be measured.
- PGAA requires a high flux neutron source with low gamma background, practically a reactor with a neutron guide. Currently it restricts the places where PGAA can be implemented, makes it immobile and expensive.

3.4.4. Applications of PGAA

The PGAA facility is a suitable tool for routine elemental analysis and for the investigation of radiative neutron capture. It can be applied in numerous different fields. The most important fields are:

- Stoichiometric investigations [Lindstrom 93]
- Hydrogen content of metals [Paul 94, Kasztovszky 00]
- Lattice water content of different materials [Lindstrom 93-2, Lindstrom 94]
- Investigations of catalysts
- Study of archaeological objects (archaeometry) [Kasztovszky 00]
- Investigation of nuclear materials (including fission material)

3.5. Coincidence

When an excited nucleus loses its excitation energy by emitting gamma photons, in most cases it goes through a series of intermediate energy levels, and emits photons with energies according to the energy difference between these levels. Such a series of gamma photons is called gamma cascade. The photons of the same gamma cascade event are in true coincidence. The process is illustrated in Figure 7.

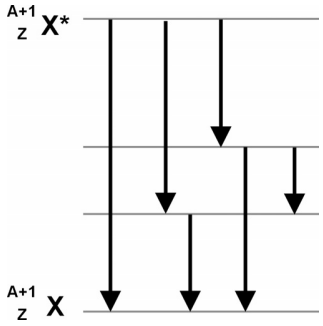

Figure 7 gamma cascade example

The true coincidence can be tested with the simple two-detector setting in Figure 8.
Two independent detectors are irradiated by a common radioisotope source that is assumed to emit at least two detectable quanta in true coincidence without appreciable time delay between the emissions of these radiations.

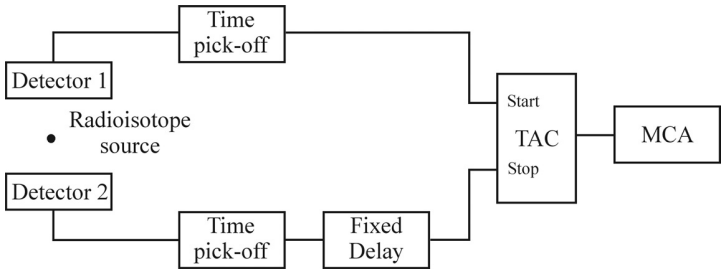

Figure 8 Simplified system to record coincidence time spectra [Knoll 00 pp667]

As a result of the spatial arrangement, there is a chance that a gamma photon hits one of the detectors, and another photon in true coincidence with the first one hits the second. The time pickoff units generate logic pulses from the detector signals. The stop line delay generates a time shift in the resulting spectra. The time-to-amplitude converter (TAC) produces an output pulse with amplitude proportional to the time interval between start and stop pulses. The maximum time of the TAC is assumed to be small relative to the average spacing between detected pulses. A schematic drawing of a time spectrum can be seen in Figure 9.

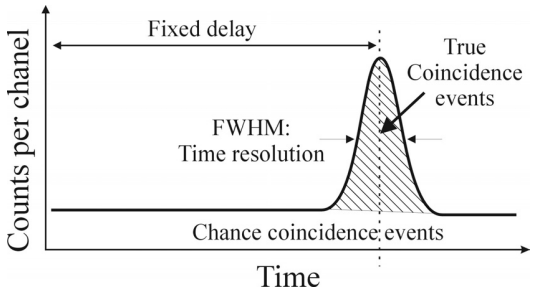

Figure 9 Expected multichannel time spectrum [Knoll 00 pp667]

The true coincidence events in a time spectrum are concentrated around a channel determined by the fix delay. If two photons from different cascade events hit the detectors within the time of the TAC, they also generate an event in the time spectrum. These so-called chance coincidence events are distributed evenly in time, so they can be separated from the true events.

Coincident detection of gamma rays (γ-γ coincidence) is a well-established technique in nuclear structure studies [Wapstra,1979]. It is well known that coincidence methods can substantially reduce interference, and hence also the complexity of spectra. The usefulness of the γ-γ coincidence technique in elemental analysis [Ehmann 91 Chapter 9.6.4 pp 302-3003] has already been demonstrated in the case of the Instrumental Neutron Activation Analysis by several authors [Meyer 87, Meyer 93, Jakubek 98, Koeberl 00]. They found it especially useful in determining Ir and Se in geological samples at a ppb level. Their main goal was to improve the sensitivity of the method by suppressing the continuous background and reducing spectral interference.

In PGAA a frequent problem is the presence of a few strong γ rays emitted by the matrix. Their Compton continuum may mask the lower energy transitions of trace elements. Two of the most "problematic" elements are hydrogen and boron. Hydrogen is dominant in biological samples and solutions. Boron is used in heat resistant glasses, and is also part of the neutron shielding around the neutron guide. Sometimes reactive samples need to be examined, and they must be irradiated in sealed borated glass containers, which greatly increases the background. Both elements have a monoenergetic γ-spectrum with no coincident cascades, so they may appear in coincidence spectra only due to random coincidence.

Recently the possibility to eliminate the hydrogen prompt gamma-ray background while increasing the signal/noise ratio in PGAA was demonstrated with scintillation detectors [Gardner 00] in a qualitative way.

3.6. Detectors

The most commonly used detectors in PGAA are the high purity germanium (HPGe) detectors:

A HPGe detector is a big germanium diode with high voltage (3-4000V) applied in the "reverse" direction, extending the depletion region almost through the whole crystal. This way the diode conducts very little current.

When a charged particle (either primary radiation or secondary particle) goes through the depleted region, it creates electron-hole pairs along its path. Their motion in the electric field applied generates the basic electric signal of the detector. The energy detected is relative to the number of electron-hole pairs, and so the voltage impulse on the detector contacts. The creation of an electron-hole pair in a semiconductor detector requires about 3 eV, while 30 eV is required for gas filled detectors. Thus the same energy of radiation causes 10 times more electron-hole pairs, resulting in better energy resolution, and also more accurate analysis.

All HPGe detectors used for the latter part of this work were of closed end coaxial type detectors, shown in Figure 10.

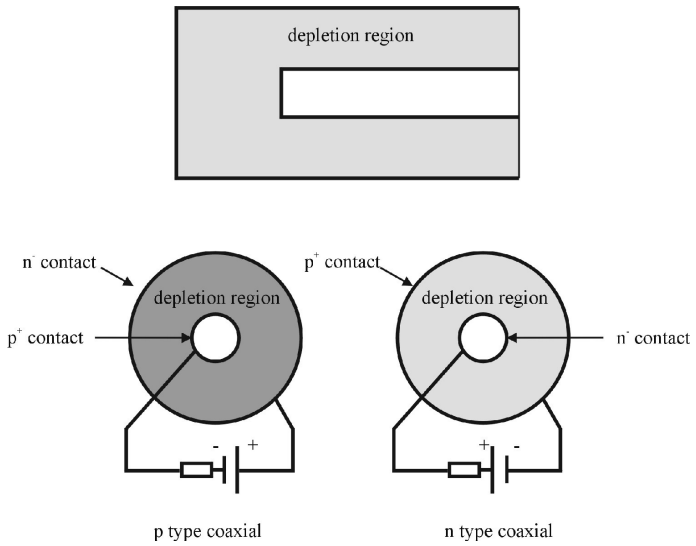

Figure 10 Closed end coaxial HPGe detector

Room temperature operation of germanium detectors is impossible because of the large thermally-induced leakage current that would induce large noise. Instead, HPGe detectors must be cooled normally to 77 K, the temperature of liquid nitrogen. Through a thermal conductor rod (cold finger), the detector has thermal contact with the nitrogen kept in an insulated dewar. The crystal must also be housed in a vacuum-tight cryostat to inhibit thermal conductivity with surrounding air. The input stages of the preamplifier are also mounted

inside the cryostat, to be cooled for noise reduction. The remaining preamplifier parts are located as close to the crystal as possible to minimize capacitance, usually incorporated as part of the cryostat module. Figure 11 shows a typical HPGe installation. More information can be found in [Knoll 00 Chapter 12]

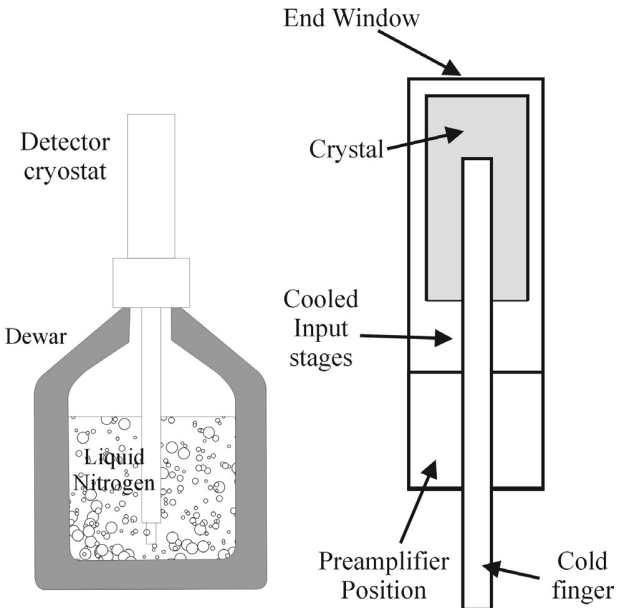

Figure 11 Typical HPGe detector installation

For the γ photon detection the photon must interact with the material of the detector to loose its energy by creating charge carriers. As illustrated in Figure 12, the following interactions are important for the detection:

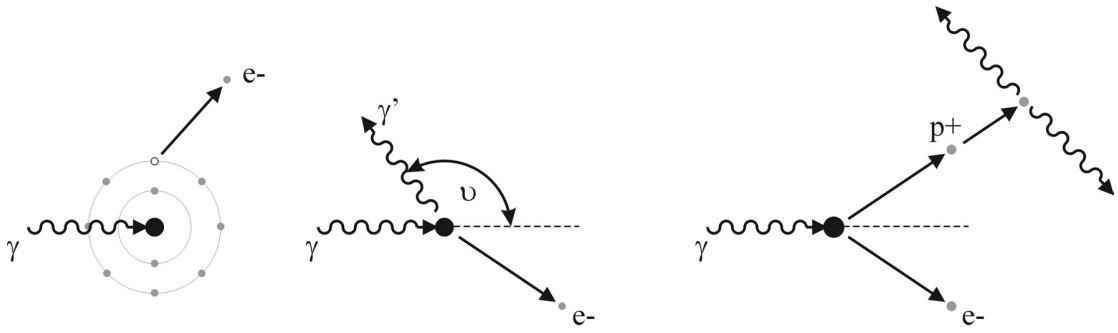

Figure 12 γ–ray interactions in HPGe detectors

Photoelectric absorption (photo effect):

The photon loses all of its energy in a single event, giving it to an electron. The electron leaves the atom with a kinetic energy equal to the energy of the gamma photon minus the electron separation energy. Then this kinetic energy is expended in creating charge carriers which generate electric signal.

The atom remains in an excited state, and can loose this excitation energy with X-ray or Auger electron emission. This interaction is dominant for low energy γ photons.

The photo effect is the ideal process to measure the energy of the original gamma ray. If a series of monoenergetic gamma rays could be detected only by the photo effect, the differential distribution of the detector signals would be a simple delta function called the full energy peak (see Figure 13)

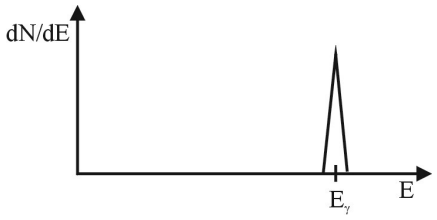

Figure 13 Detector response function to the photo effect (ideal detector)

Compton scattering:

The photon can't lose all of its energy at once, instead it gives only a part of its energy to an electron, then the scattered lower energy photon can participate in a series of similar reactions. The energy of the Compton-scattered photon can be calculated using the following equation:

$$E'_\gamma = \frac{E_\gamma}{1 + \frac{E_\gamma}{m_0 c^2} \cdot (1 - \cos\vartheta)}$$

where m_0 is the electron mass, c is the speed of light in vacuum, E_γ is the incoming photon energy, ϑ is the angle between the incoming and outgoing gamma photons.

In Compton-scattering, the electron takes on the difference of the incoming and outgoing γ-ray energies. If $\vartheta \cong 0$ then $E'_\gamma \cong E_\gamma$, and the energy of the electron is close to 0. If $\vartheta \cong \pi$, the incident gamma photon is backscattered toward its direction of origin, while the electron recoils along the direction of incidence. This case represents the maximum energy that can be transferred to an electron in a single Compton interaction. Under normal circumstances, all scattering angles will occur in the

detector. Therefore, a continuum of energies is transferred to the electron, ranging from zero up to the maximum (see Figure 14).

For large gamma energies, the E_C energy gap between the maximum Compton recoil electron energy and the incident gamma-ray energy is constant:

$$E_C = \frac{E_\gamma}{1 + \frac{E_\gamma}{m_0 c^2} \cdot (1 - -1)} \cong \frac{m_0 c^2}{2} = 0.256 MeV$$

Figure 14 shows the response function with Compton-scattering.

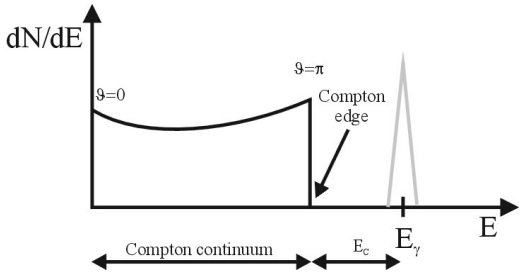

Figure 14 Response function when Compton scattering is added to Figure 13

Pair production:

This reaction is energetically possible only if the gamma energy is greater than twice of the electron mass (2*511 keV). Within the range of the Coulomb force of the nucleus, the gamma ray completely disappears creating an electron (e-) – positron (p+) pair. Then the kinetic energy of both particles is expended in creating charge carriers, but the positron at the end of its track will annihilate and create two 511 keV gamma photons. One or both of this photons may leave the detector without creating charge carriers within the time resolution of the detector. In this case, extra peaks will appear in the response function. One with an energy of 511 keV, and another at 1022 keV below the full energy peak. They are called single and double escape peaks (see Figure 15).

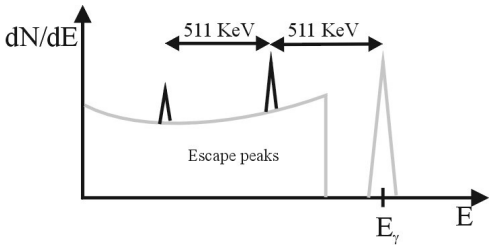

Figure 15 Response function when pair production is added to Figure 14

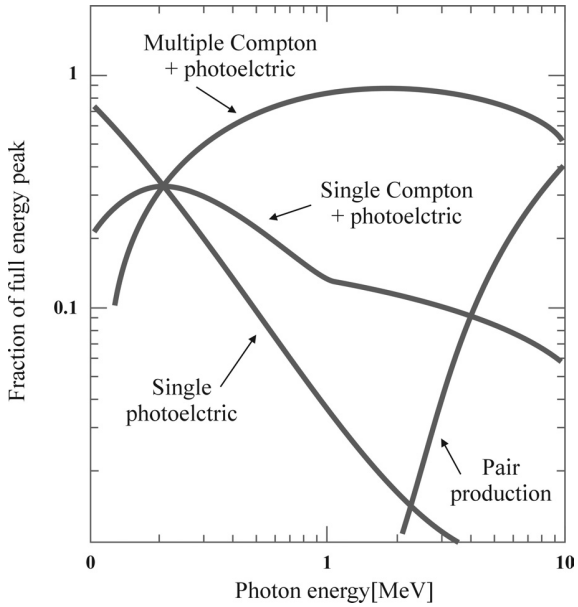

Figure 16 Fractions of the full energy peak contributed by different interactions in a 6 cm X 6 cm coaxial HPGe detector. [Knoll 00 pp 430]

The relative probability of the different interactions depends on the gamma energy, as shown in Figure 16. At low energies the photo effect is dominant, while from a few hundred keV the Compton scattering becomes dominant. Pair production is irrelevant under 2 MeV, but has 40% contribution to the full energy peak at 10 MeV.

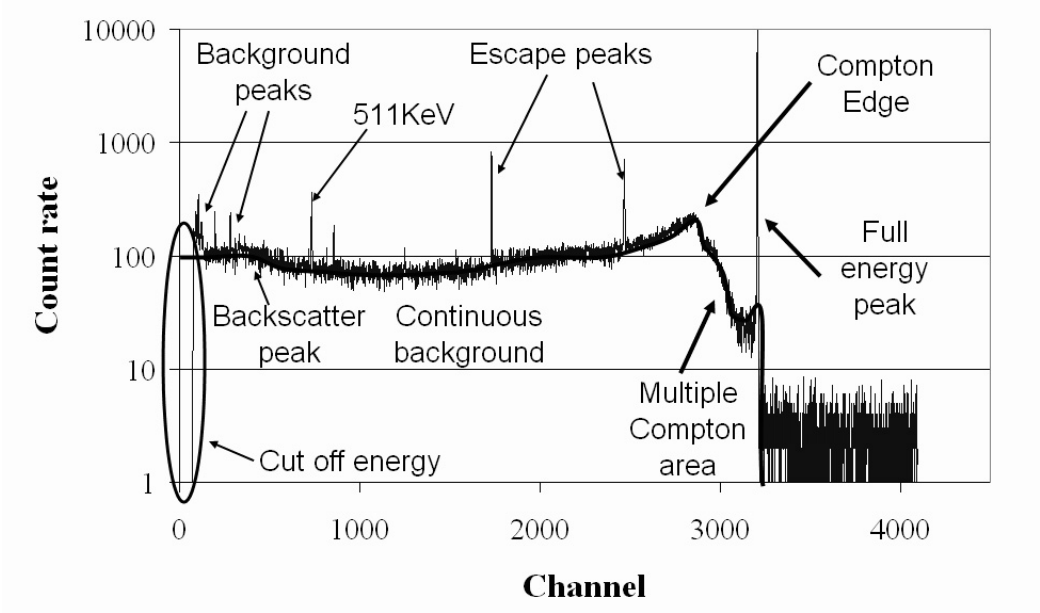

Figure 17 Real detector response function to γ–rays from H(n,γ) reaction

Figure 17 shows the response function of a real HPGe detector for the gamma photons from the (n,γ) reaction of hydrogen. This reaction is a monoenergetic source, not considering the room background.

All parts of the response function discussed above can be identified easily. But there are also undiscussed parts:

1 If the Compton scattered photon goes through more Compton scatters before escaping, the detector collects the sum energy. Some of these events can appear in the area between the Compton edge and the full energy peak. In this area, called **multiple Compton area,** the events mainly come from multiple Compton scattering.
2 The detector crystal is unavoidably surrounded by other materials that have a measurable influence on its response. At the least, the detector is surrounded by the cryostat elements (see Figure 11).
   – A part of the **background peaks** (mostly X-rays) is coming from the room background, another part comes from the (n,γ) reactions in the material surrounding the detector.
   – If the gamma-ray source emits positrons or pair production happens in the surrounding material, additional **511 keV** annihilation peak appears in the spectrum.
   – Gamma-rays of the source that first interacted by Compton scattering in one of the materials surrounding the detector can cause an unusually wide peak in the range of 0.2-0.25 MeV called **backscatter peak**.
3 **Cut off part**: This effect is caused by the settings of the electronics. The threshold of the instrument is intentionally increased to reduce the number of events from noise and low energy X-rays.

The detector has three parameters, important for later parts:

1 **Relative efficiency** of the detector is given as the photo peak efficiency relative to a 3 in **X** 3 in (7,62 cm **X** 7,62 cm) cylindrical NaI scintillation crystal efficiency for the 1332 keV peak of ^{60}Co with a detector-target distance of 25 cm. This efficiency can be determined simply by measuring the photo peak areas from both detectors using the same ^{60}Co source at a distance of 25 cm.

2 The **Energy resolution** of the detector is characterized by the full width at half maximum (FWHM). The definition of the FWHM is illustrated in Figure 18. The energy resolution can be specified in two different ways: as the FWHM at a given peak (eg.: 1332 KeV of ^{60}Co) or as percentage of $R=FWHM/E_\gamma$ [%] for a given energy.

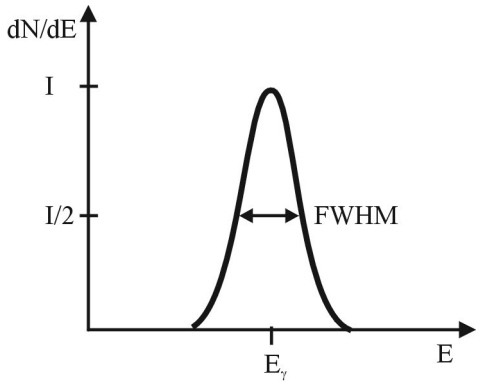

Figure 18 Full width at half maximum (FWHM) definition

3 The **total to peak ratio** *r* is the ratio of the total amount of events A_{total} detected from a monoenergetic source (peak and all parts of its background together) and the events detected in the full energy peak from that source A_{peak}.

$$r = \frac{A_{total}}{A_{peak}}$$

The total to peak ratio greatly increases with the gamma energy.

4. The PGAA-NIPS facility at the Budapest research reactor

4.1. The reactor, the cold neutron source and the neutron guides

The reactor was constructed in 1959 with a thermal power of 5 MW. Between 1986 and 1992, the reactor was reconstructed, it was upgraded to 10 MW thermal power. One of the tangential beam tubes was prepared to install a cold neutron source with a neutron guide system. A 15m x 27m guide hall was also constructed for housing the three planned neutron guides with the connected experimental facilities. Because of financial difficulties, the installation of the cold neutron source (CNS) was delayed, but the guides and applications were started up with thermal neutrons. In 2001 the cold neutron source was installed and the neutron guides were mostly replaced by supermirrors.

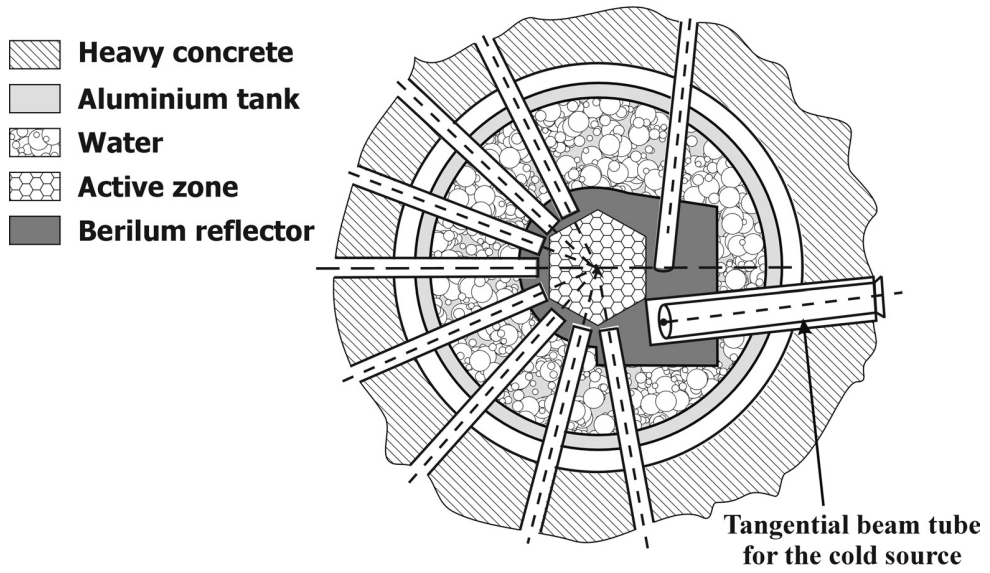

Figure 19 Reactor zone with radial and tangential beam tubes

The 10 MW reactor has a thermal neutron flux of 2.2 * 10^{14} n/cm^2 s and a fast neutron flux of 1.0*10^{14} n/cm^2 s in the core. The tank type reactor is cooled and moderated by light water. The active zone is situated in a cylindrical aluminum alloy tank with a height of 5685 mm and a radius of 2300 mm. The active zone consists of 239 Russian made, 36% enriched uranium fuel rods positioned hexagonally with a lattice pitch of 35 mm. The core is surrounded radially by a solid beryllium reflector. The reactor is equipped with two boron-carbide safety and shim rods, and has a stainless steel rod for the purpose of automatic power control. The

schematic cross-section of the reactor is shown in Figure 19. The tank is surrounded by a heavy concrete biological shielding in a 600 m^2 rectangular semi hermetical reactor hall.

The reactor has 51 vertical and 10 horizontal (8 radial and 2 tangential) irradiation tubes allowing radioisotope production and a large variety of nuclear applications. The reactor and the experimental facilities form the Budapest Neutron Centre (BNC). The BNC consists of the following instruments built around the reactor and the guides [BNC 00]: **PGAA**-NIPS facility [Belgya 02], **RNAA**: neutron activation analysis with a pneumatic rabbit system installed in one of the vertical tunnels, **PD** powder diffractometer, **SANS** small angle scattering spectrometer with XY detector called "Yellow Submarine", **TASC** triple-axis spectrometer, **RAD** Dynamic and static n/γ radiography, **BI** biological irradiation channel, **FB** filtered beam (planned), **REFL** Neutron reflection measurements

The overview of the neutron guides and the deployment of the instruments can be seen in Figure 20.

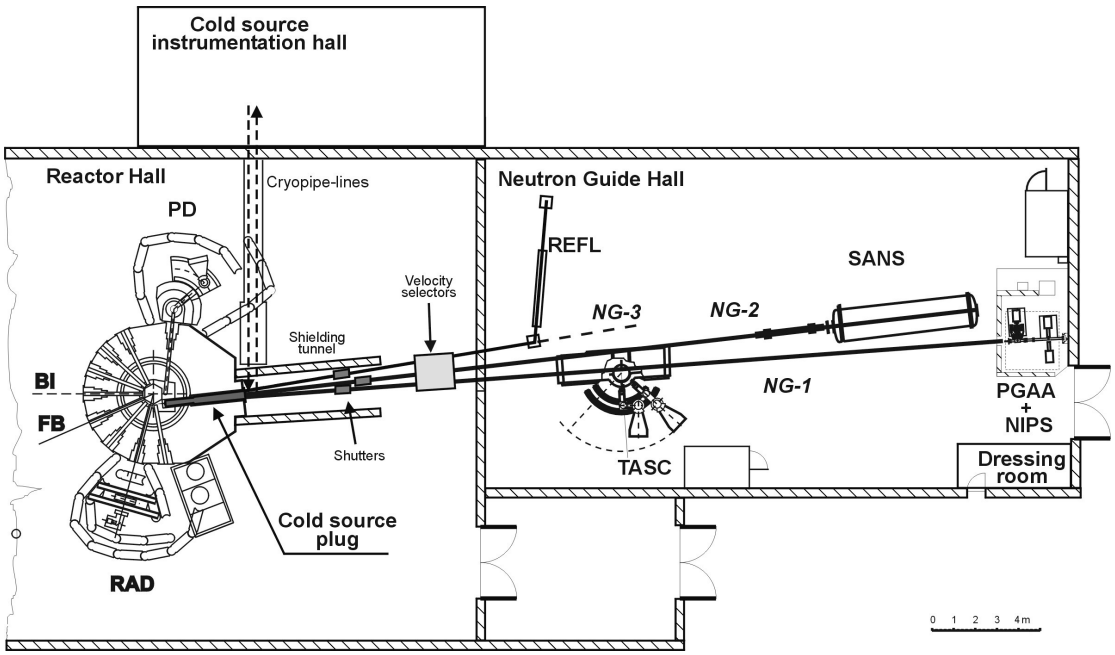

Figure 20 Reactor hall, guide hall and the position of the instruments.

The cold source is plugged into the tangential beam tube shown in Figure 19. The special double walled moderator cell is positioned at the end of the tube inside the beryllium reflector, close to the maximum of thermal neutron distribution (see Figure 5). The cell is filled with 400cm^3 of liquid hydrogen. The moderator cell is inside an explosion proof vacuum case and is cooled by 14 K He gas. The He refrigerators and the hydrogen buffer are

positioned in the cold source instrumentation hall. The plug and the cooling system are connected by a special transfer line (cryopipe-line).

Three evacuated supermirror neutron guides (NG-1, NG-2 and NG-3) with independent beam shutters are connected to the plug. The angles between guides NG-1 - 2 and NG- 2 - 3 are 1.5 and 2 degrees respectively.

The neutron guides have a curvature to avoid gamma background caused by the direct view of the reactor core. The 35-meter long NG-1 guide has a curvature of 5000 m, and a cross section of 100 mm x 25mm. Heavy and normal concrete, lead and boron loaded paraffin bricks surround the guides to provide biological and neutron shielding for the experimental instruments. The guides are detailed in [Rosta 02].

4.1.1. Short history of the PGAA-NIPS facility

The PGAA studies at the Budapest research reactor started in 1993. After two years of careful planning and designing, the first PGAA measurement with the Compton suppressed spectrometer at the end of NG-1 thermal guide of the upgraded Budapest research reactor was performed in 1995. After the initial measurements and the tuning of the electronics and measurement techniques, the development of the HYPERMET-PC data processing software [Fazekas 97] was started. With the suitable background, the PGAA data library could be established: Most of the elements were measured and catalogued from 1997 till 1998 [Révay 98]. The work is still going on to enhance the library [Molnar 00, Révay 01].

Gamma-gamma coincidence studies were started in 1998. The first experiments were made using the HPGe detector and the target chamber of the Compton suppressed spectrometer. These preliminary measurements helped the planning of another PGAA facility suitable for gamma-gamma coincidence and other measurements.

The real change came in 2001 with the installation of the cold neutron source and the reconstruction of the neutron guide. These modifications increased the neutron flux approximately by a factor of 20 (from $2*10^6$ to $5*10^7$). According to the plans, a new facility, the Neutron Induced Prompt gamma Spectroscopy (NIPS) was installed at the end of NG-1 next to the existing Compton suppressed spectrometer facility.

Both facilities can be operated at the same time. The following sections describe the current situation.

4.2. PGAA-NIPS experimental area

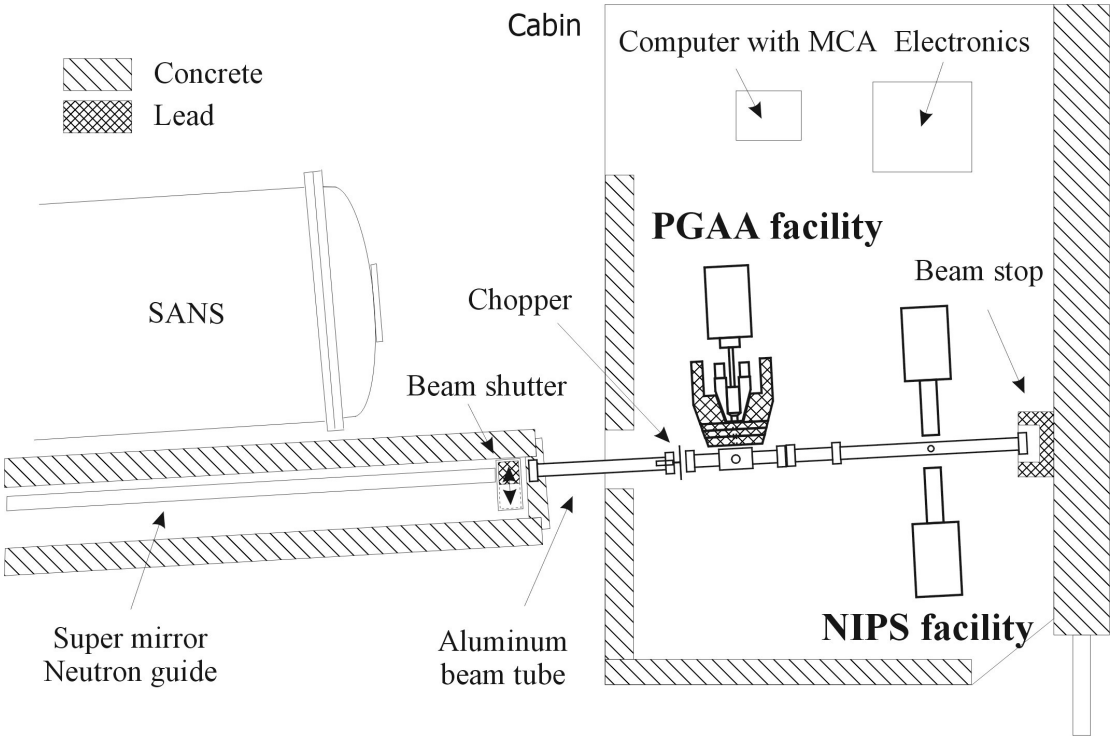

Figure 21 Overview of the PGAA beam port at the Budapest research reactor

Figure 21 shows the schematic drawing of the PGAA-NIPS facility [Belgya 02] at the end of guide NG-1. The 3 m x 6 m experimental area is enclosed in a cabin covered with iron screening to protect the detectors and the electronics from outer electromagnetic noise. The 35 m long supermirror neutron guide, which has a cross section of 10 cm x 2.5 cm, ends outside the cabin. An evacuated aluminum tube guides the neutron beam into the cabin. This tube contains highly enriched ^{6}LiF loaded polymer collimators on both ends (see Figure 22), which divide the beam into an upper and a lower beam with sizes of 2 cm x 2 cm. The two beams can be operated separately with a double pneumatic beam shutter positioned at the end of the neutron guide. The upper beam is used for the conventional Compton-suppressed PGAA analysis [Belgya 96; Molnár 97], while the lower beam passes through under the Compton-suppressed target chamber and enters the neutron induced prompt gamma spectroscopy (NIPS) target chamber. The latter is designed to provide diverse experimental conditions, including those suitable for γ-γ coincidence experiments.

Figure 22 shows the details of the PGAA beam port. The top and side view of the Compton suppressed spectrometer and the NIPS facility are shown. The two target chambers and the

beam tubes are made of aluminum lined with ^{6}Li loaded polymer, and can be evacuated or filled with ^{4}He or other gaseous atmosphere to decrease the background caused by the interactions of neutrons with the nitrogen in the air. An optional beam chopper can be mounted before the PGAA target chamber on either the upper or the lower beams.

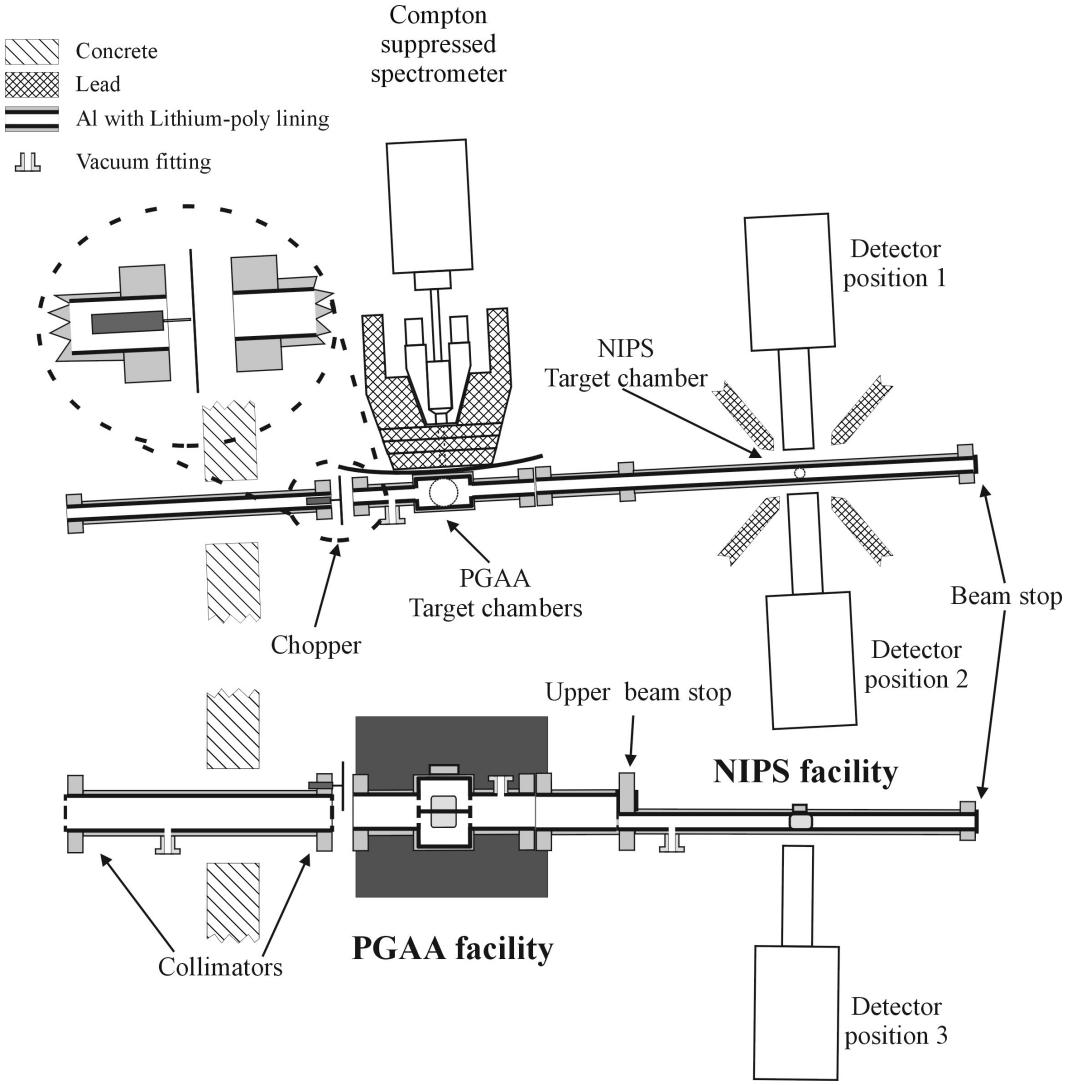

Figure 22 detailed view of the Compton suppressed spectrometer and the NIPS facility

4.3. The PGAA facility

The target position of the PGAA facility is at a distance of 1.5 m from the beam shutter, and 30 cm from the chopper. The neutron beam can be further collimated at the beginning of the target chamber with a series of highly enriched ^{6}LiF loaded polymer collimators. The upper beam stop is made of highly enriched ^{6}LiF loaded polymer. It is surrounded by lead blocks and is positioned at a distance of 45 cm behind the target position. The second beam passes through under this chamber, and is separated by a ^{6}LiF loaded polymer sheet. The average thermal equivalent neutron flux[1] at the sample position is $5*10^{7}$ n/cm^{2} s, measured by gold foil activation, while the effective temperature of the beam is about 30 K. The observable target volume is about 10 cm^{3}. Solid, powder, liquid or gas samples can be put in the target chamber. Powders and liquids can be measured in sealed FEP Teflon bags or vials, gas samples must be put into pressure containers. Solid samples are typically fastened by teflon strings onto an aluminum frame that can be put into the beam perpendicular or at 30 degrees to the beam direction. Larger targets can also be measured by removing the whole target chamber section of the beam tube. The target chamber is lined with 3 mm ^{6}LiF loaded polymer for neutron shielding and has a 0.5 mm thick aluminum window. It can be evacuated or filled with gas.

The gamma radiation emitted by the sample goes through the polymer and the 0.5 mm aluminum window, and three 3.5 cm thick lead disk collimators with 2.4 cm inner diameter before it reaches the HPGe detector. When all three disks are in position, the minimum distance of the detector face and the target centre is 235 mm. The n-type closed end coaxial high purity germanium (HPGe) detector has an energy resolution of 1.8 keV, and a relative efficiency of 25% at 1332 keV (^{60}Co). It is surrounded by a BGO scintillator guard detector annulus. The annulus consists of octally split segments, and two back catcher crystals behind the detector, around the cold finger. The detector assembly is surrounded by 10 cm thick lead shielding. A schematic drawing of the detector assembly is presented in Figure 23. The parameters of the PGAA facility are detailed in Appendix A.

---

[1] Thermal equivalent neutron flux is a measure independent from the energy distribution of the beam; it indicates the required flux of thermal neutrons which would cause the same counting rate as the heterogenic beam.

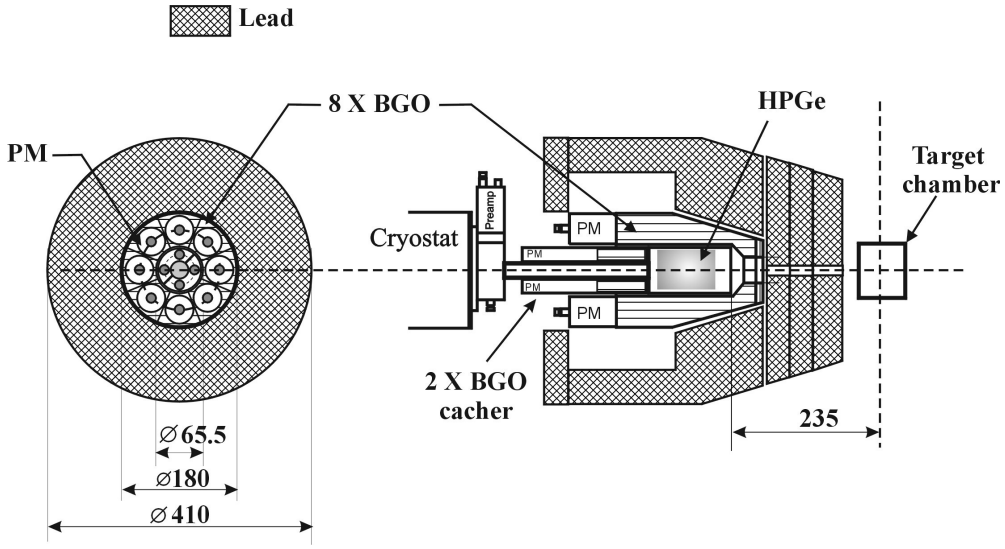

Figure 23 The Compton suppressed spectrometer

The detector assembly described above can be used for three different kinds of measurements:

1. Singles mode. The signals of the Ge detector are collected without any gating.

2. Compton suppressed mode. An anticoincidence relationship is required between the HPGe and the BGO annulus. In this case the system collects only those events when the HPGe is fired without firing any segments of the BGO. These γ photons have most probably lost all of their energies in the HPGe detector, so their detector signal belongs to the full energy peak. The rejected events, when the HPGe detector is fired together with any segment of the BGO annulus are mostly caused by γ photons Compton scattered from the HPGe to the BGO. They would belong to the Compton background.

Because the solid angle is close to 4 π, the suppression is very efficient. For describing the quality of the suppression the following parameter is used:

$$CSF = \frac{A(1332\,keV)}{A(1040-1096\,keV)}$$

where „A (1332 *keV*)" is the area of the 1332 keV peak, and „A(1040-1096 *keV*)" is the integral of the Compton plateau from 1040 keV to 1096 keV in a ^{60}Co measurement. With our spectrometer and electronics this factor can be as high as 11, although in singles mode the same factor is around 2. So the spectrometer has an enhancement factor of about 5 at 1332 keV. The enhancement is about 40 at 7 MeV. In Figure 24 a part of the singles and the Compton suppressed spectra of the same hydrogen containing sample are shown. The area of the hydrogen peak is the same in both cases, but the hydrogen Compton plateau is lower, the enhancement factor is ten.

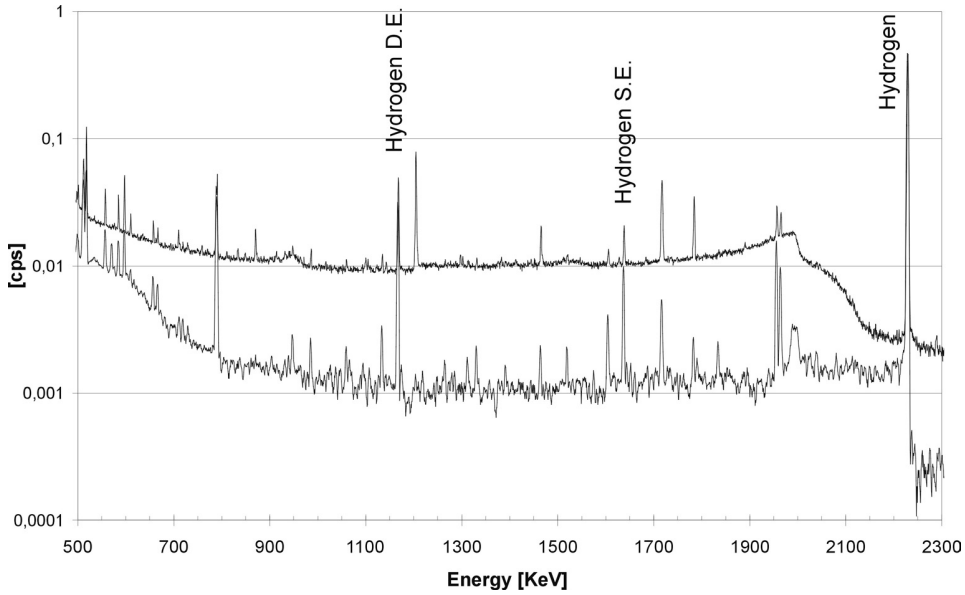

Figure 24 Spectra of Singles mode (above) and Compton suppression (below) spectra of Hydrogen PGAA

3. Annihilation-pair mode. This setup takes advantage of the segmentation of the BGO. A triple coincidence relation is required between the HPGe detector and two opposite segments of the BGO to select only those events when a γ photon creates an electron-positron pair in the HPGe detector, and the two 511 keV γ photons caused by the annihilating positron are captured by the two BGO segments. If an energy gate is put on the BGO segments, this method can decrease the background by 100-1000 times. This method can be used only for high energies. Due to its low efficiency, it is not in general use.

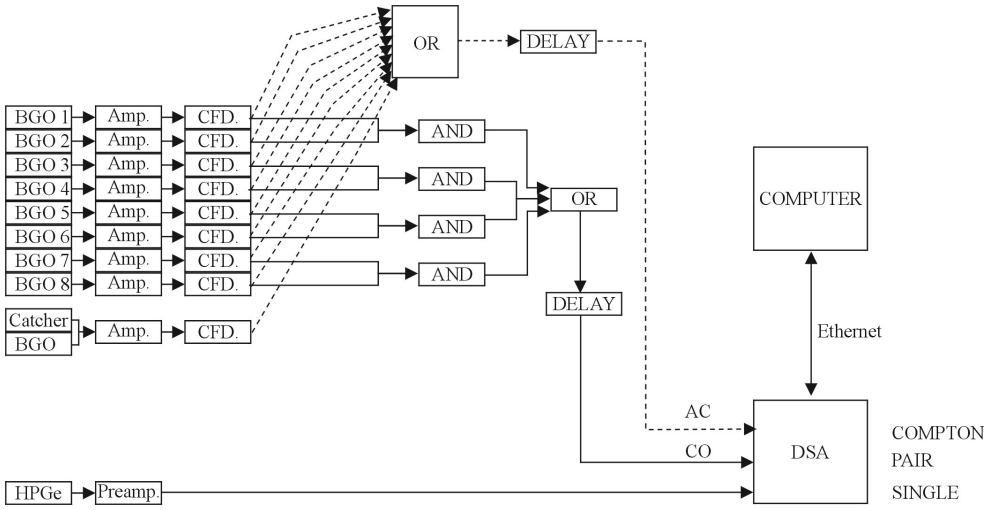

Figure 25 Compton suppressed spectrometer electronics block diagram

With appropriate electronics all three measurement setups can work at the same time. Figure 25 shows the electronics for all three. Through a preamplifier and an amplifier the HPGe detector sends signals to a 16k analogue-digital converter (ADC) in all three cases. The amplified signals of the 8 BGO segments and the catcher crystals are connected to constant fraction discriminators (CFD).

In the case of the Compton suppressed setup, the “OR” relation of the 9 CFD signals is used as anticoincidence (AC) gate for the ADC. The gating signal is delayed in order to be synchronised with the HPGe signal. With this circuit the ADC rejects the HPGe signal if it comes together with a signal from any BGO segment.

In the annihilation-pair mode, the catcher is not in use, and the CFD signals of the opposite BGO segments are in “AND” relation. The signals of the four AND gates are in “OR” relation. This OR signal serves as coincidence gate for the ADC. The gating signal is delayed in order to be synchronised with he HPGe signal. With this gate the ADC converts only those HPGe signals which come together with two signals from opposite BGO segments. Energy gates can be put for the sum signal of the BGO segment pairs, which means an energy of 1022 for the two 511 keV gamma photons.

The ADC is connected to a computer with an S-100 MCA board. A software application made by Canberra collects the events into a .MCA format file.

4.4. An industrial PGAA application to demonstrate the matrix effect

Series of measurements with an inactive tracer were carried out at our institute to analyze the mixing process of glass furnaces, which is important for the technologists of the customer. On the customer's request, the final conclusions about the glass furnaces could not be presented here. But the method of the measurement and demonstration of the matrix effect is allowed to be here.

For similar investigations, radioisotope tracing have been widely used [Földiák 72]. The most commonly used tracer isotopes were ^{51}Cr or ^{24}Na. In the present case, calculations showed that because of the big size of the furnaces, the radioisotope tracing would require such a high activity of tracer that can not be applied because of the radiation safety rules. Also, the handling of radioisotopes would require special arrangements, and there is a considerable risk of contaminating the device or the product. A safe solution is the use of an inactive tracer, and the PGAA measurement of the samples. An additional advantage of this solution is the possibility to repeat the measurements even years after the samples were taken.

The measurements of samples of glass containing boron are good examples for the so called matrix effect, that is, when signals from a component of the sample can not be determined due to interferences with other components of the sample. These difficulties are usually associated with very complex spectral interferences, extremely large capture cross section of a component, or just a large amount of the matrix component in the total sample.

4.4.1. Inactive tracing of glass melting furnaces

Glass melting furnaces work around the clock, processing several tens of tons of ingredients into glass. Knowledge of the flow conditions inside such a device has a big importance for the industrial technologists. This can be investigated indirectly by injecting a tracer in the same instant as the ingredients, and taking samples from the outcoming melted glass at certain times. From the samples, the concentration of the tracer can be determined, and then the technologist can reconstruct the flow conditions. The process is shown in Figure 26.

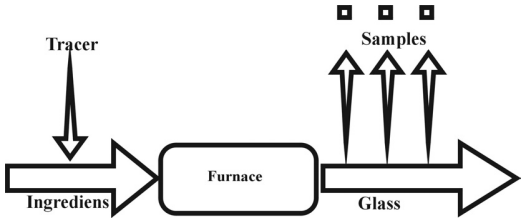

Figure 26 Glass furnace tracing process

4.4.2. Choice of the tracer

Important criteria in tracer selection were that it should not affect the technology, nor change the parameters of the glass produced, and furthermore, it had to have a great neutron capture cross section. Great cross section elements are for example: B, Cd, Sm, Gd, Hg. Cd and Hg are toxic, so their usage is undesirable. The PGAA measurement of the untraced glass showed that glass contains all these elements in 1-5 ppm of concentration. The selected tracer must be introduced into the furnace in a chemical and physical form similar to the form of the ingredients to make sure that it melts and moves similarly. For PGAA, two kinds of glasses have special importance: normal (containing boron only in 1-5 ppm concentration), and borosilicate glasses (containing about 5 % boron). The high boron concentration makes tracing with boron impossible, and its high neutron capture cross section creates a very high spectral background, making the spectrum evaluation difficult.

Due to preliminary investigations, gadolinium in the form of gadolinium-oxide was selected for the borosilicate glasses. For normal glasses, the use of this expensive material is not necessary, boron can also be applied in the form of boric-acid.

Preliminary calculations showed that 10-100 ppm of tracer is enough in each case.

4.4.3. Evaluation and results with the Compton suppressed spectrometer

For boron tracer the boron concentration was determined by evaluating the single existing boron peak at 478 keV. This peak appears in the spectrum as a characteristically wide peak (see Figure 27). The widening is due to the Doppler shift of the emitted gamma ray caused by the recoil of the lithium nuclei arising from the $^{10}B(n,\alpha)^{7}Li$ reaction.

Table 3 The gadolinium peaks, applicable for the concentration determination, the sensitivity for these peaks, and their spectral interferences

E [keV]	sensitivity[cps/mg]	Interferences
42	62	X-ray lines
79	31	X-ray lines
89	11	X-ray lines
182	51	B Compton-background
199	14	B Compton-background
944*	7,2	2•478 keV B sum peak
1184*	2,3	1186 keV Gd
1186*	6,3	1184 keV Gd

In the case of gadolinium tracer used for borosilicate glasses, Table 3 shows the gadolinium peaks which can be used for determining concentration, the sensitivity of the Compton

suppressed spectrometer for these peaks, as well as the spectral interferences disturbing their evaluation.

The most convenient way would be to use the 182 or the 199 keV peaks, because they are not in the region of X-ray photons (see Figure 17), and the detector has a high efficiency for them. The problem with the evaluation of these peaks is the very high background of boron. For lower concentration samples these two peaks completely disappear in the statistical fluctuation of the background. Finally, the 944 keV, the 1184keV and 1186 keV lines (marked with * in Table 3) were used for the evaluation because they are present in the spectra of all samples. An example of such a spectrum can be seen in Figure 27, in which the peaks indicated above are marked. Due to the high rate of boron photons there is a high chance of detecting two 478 keV photons within the charge collecting time of the detector, these events create a random coincidence peak at $2 \cdot 478$ keV. The 944 keV gadolinium peak is on the leading edge of this extra peak, shown as enlarged insert in Figure 27. This steep slope makes the evaluation of the peak more difficult. As also enlarged in Figure 27, the 1184 and 1186 keV peaks are so close to each other, they can only be evaluated together.

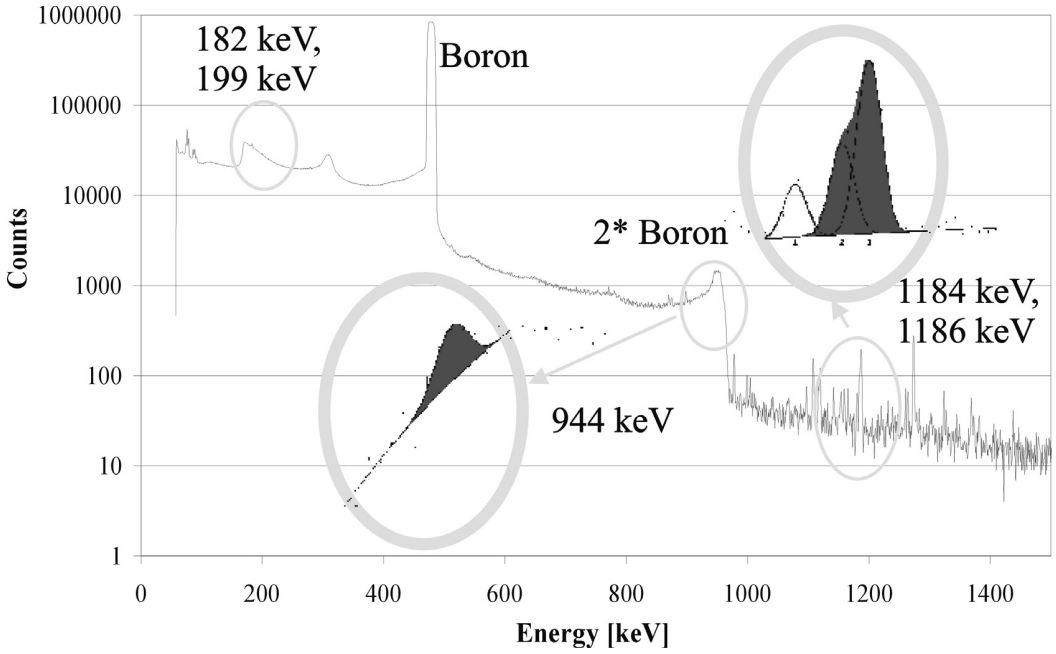

Figure 27 gadolinium peaks in the borosilicate sample measured with the Compton suppressed spectrometer

4.5. The neutron induced prompt gamma spectroscopy (NIPS) facility

The NIPS facility [Belgya 02] is the second experimental station at the PGAA beam port (see Figure 21). The NIPS target chamber is positioned about 2.6 m downstream from the beam shutter, and about 1 m from the PGAA target chamber. As shown in Figure 22, the NIPS facility uses the lower half beam. A square aluminum tube with an outer cross section of 5 cm x 5 cm and a wall thickness of 3 mm encloses the neutrons as they travel from the collimator to the beam stop. This tube section can be evacuated separately from the target chamber of the Compton suppressed spectrometer. For neutron shielding, its inner walls are lined with a 3 mm thick layer of ^{6}LiF loaded polyethylene sheet. The collimated neutron beam has an approximately 2 cm x 2 cm cross section at the target position, with a thermal equivalent neutron flux of 3 x 10^{7} n/cm^{2} s.

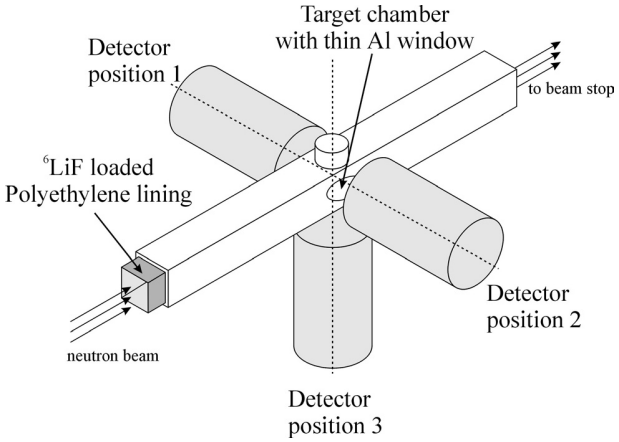

Figure 28 NIPS target chamber and detector positions [Belgya 02]

It is designed for studying sample radiation with a variety of detector setups, like the double or triple gamma coincidence. The thin aluminum-windowed target chamber is lined with 2.3 mm thick sheets of highly enriched ^{6}LiF loaded polyethylene to protect the detectors from scattered neutrons. It can hold samples as large as 1.5 cm in diameter and 3.5 cm in length. The small size of the target chamber allows us to use up to three closely positioned γ-ray detectors at one time, as shown in Figure 28. All of them can be placed perpendicular to the neutron beam, one at each side, and one below the target chamber. The detector faces can be as close as 2.5 cm to the center of the target. Detectors can be either semiconductor or scintillation detectors. At present we can equip this experimental station with two coaxial HPGe detectors and a third planar HPGe detector, or with one HPGe and two fast BaF_2 detectors for fast timing experiments. The parameters of the NIPS facility are collected in APPENDIX B.

4.6. Flux and neutron spectrum measurements

The thermal equivalent neutron flux was measured with gold foil activation. The same method was used as in the case of conventional neutron activation analysis: a very thin gold foil was irradiated in the beam. The number of activated gold atoms, which is proportional to the neutron flux, can be determined by measuring the γ-rays emitted by the foil.

Gold foil is ideal because it is monoisotopic, and its cross section and half life are known very accurately. If the sample is thin enough, the attenuation of the beam and the gamma self absorption can be neglected.

Neutron spectrum was measured with the chopper using time of flight technique [Révay 02]. The opening was set to 1 mm and a standing horizontal slit was inserted into the beam. The chopper was operated at a frequency of 70 Hz, thus the neutron beam was cut into 60 μs packages. Due to their velocity dispersion the neutron packages spread on the way from the chopper to a boron target. The prompt gamma photons were counted and recorded in multichannel scaling mode with 10 μs dwelling time. The obtained spectra were transformed into wavelength spectra. The wavelength spectra of both the cold beam and the thermal beam (when cold source was not operating) are shown in Figure 29. The total number of counts was 20 times larger in the case of the cold beam. The calculated average temperature was 100 K for the thermal beam, and 30 K for the cold beam.

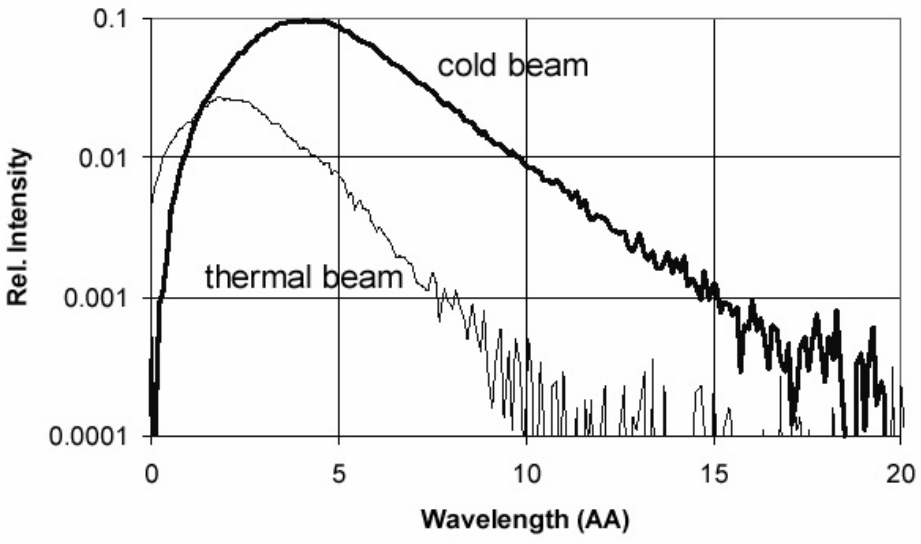

Figure 29 Wavelength spectra of the cold and thermal beams measured with time of flight technique in the Compton suppressed spectrometer target chamber [Révay 02]

4.7. Peak analysis with the HYPERMET-PC program

In neutron capture γ-ray spectroscopy, one has to cope with the complexity of spectra and the problems of energy and efficiency calibration over a wide energy range. Beside the large number of peaks with superimposed Compton backgrounds, the overall presence of complex multiplets and escape peaks with nonstandard underlying background pose problems which are usually not present in the case of simple radioactivity spectra. Hence a highly flexible computer program is required for the evaluation of (n,γ) spectra.

The original HYPERMET code was developed in FORTRAN by Phillips and Marlow [Phillips 76] in the early seventies at the Naval Research Laboratory, Washington D.C. for automatic and efficient analysis of multichannel pulse-height spectra using a high-speed mainframe computer.

In the nineties PCs became available which are fast enough to run the HYPERMET code with some modifications. The progress of object-oriented programming languages for PCs has motivated the development of an interactive version with a user-friendly graphics environment and built-in database. HYPERMET-PC is an interactive DOS mode program developed at our department [Fazekas 97] on C++ developer's platform. The work has continued for years [Fazekas 98], and some additional new modules have been developed recently [Révay 01].

With this application, almost all steps of (n,γ) spectra evaluation can be done, including the efficiency, and nonlinearity calibration, automatic peak fitting, and the nuclide identification.

5. Experimental work

This chapter contains my work in logical order.

- The first subchapters *(Chapter 5.1 and 5.2)* contain the details of the γ-γ coincidence experimental setup realized at the NIPS facility.
  - Detector setup and
  - Coincidence electronics
  - Data acquisition for later off line processing
  - Off line data processing with detailed description of the conventional peak-to peak coincidence.
  - The γ-γ regional coincidence method is an advancement of the conventional peak-to peak data processing. It is presented only in Chapter 5.6 to follow the logical order.

- The later subchapters present a series of measurements I have performed; from the most basic test with a radioactive source to a coincidence realization of the industrial application (presented in Chapter 4.4):
  - A simple peak-to-peak coincidence measurement with ^{60}Co to determine the time resolution of the system, and to demonstrate the possibility of simplifying the spectra. *(Chapter 5.3)*
  - A PGAA measurement on a chlorine sample to determine the FWHM of the time peak for the peak-to peak coincidence method for different cases (it is also a good illustration of the time walk), and to demonstrate how the results are in connection with the decay scheme of a nucleus. *(Chapter 5.4)*
  - The total-to-peak ratio of a HPGe detector as the function of the γ energy determined using γ-source and (n, γ) measurements to provide the foundation of the idea of the regional coincidence method. *(Chapter5.5)*
  - Measurements of a cobalt-chloride sample in boron environment to compare the regional coincidence method with the Compton suppressed spectrometry. *(Chapter 5.7)*

– A series of measurements with cobalt-chloride in boron environment to create a calibration curve and to prove that the regional γ-γ coincidence method is applicable for analytical work. *(Chapter 5.8)*
– A series of measurements of gadolinium traced borosilicate glass to prove that the regional γ-γ coincidence method can eliminate the matrix effects in real samples as well. *(Chapter 5.9*)

As the NIPS facility was designed according to the results and needs of my experiments, the measurements of this chapter are not in calendar order. Some measurements were made prior to the construction of the facility. The descriptions of these measurements contain details of the circumstances they were performed in. The others were performed with the same settings (standard setup detailed in the first subchapters).

5.1. The γ-γ coincidence experimental setup and data acquisition

Figure 30 shows the schematic drawing of a γ-γ coincidence measurement. The signals of the detectors are processed with special electronics. The data is collected by a computer into a list file. The file is processed offline after the measurement. This enables the determination of the optimal gate conditions to improve the sensitivity for a selected element or to suppress another.

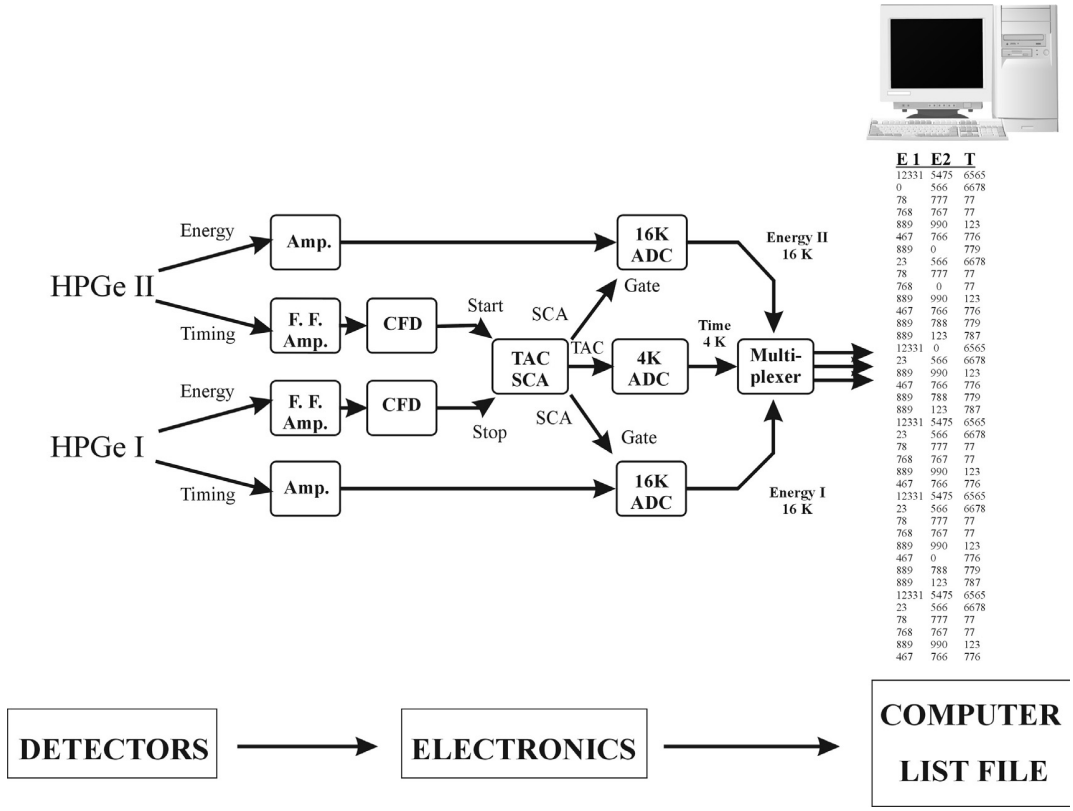

Figure 30 Schematic drawing of a γ-γ coincidence measurement

For the measurements detailed in the latter chapters, mostly the following detectors and electronics (standard setup) were used at the NIPS station:

5.1.1. Detectors

Two n-type coaxial HPGe detectors were used for the standard setup (see Figure 31). The larger detector (HPGe–I) had 30% efficiency compared to a 3" x 3" NaI detector and 1.8 keV resolution at 1332 keV γ-ray energy of ^{60}Co calibration source. The smaller detector (HPGe–II) had 15% efficiency and 1.9 keV resolution. The HPGe–II detector was placed horizontally

at position 1, at a distance of 2.3 cm from the Al tube, and HPGe–I vertically at position 3, about 0.6 cm from the Al tube.

This 90° setup was chosen because a 180° setup (when detectors are on the opposite sides of the tube) has more significant back-scatter. Lead blocks of 5 cm thickness were used around the crystals as gamma shields, and plates of 1.5 mm thick lead were placed between the detectors and the tube to further decrease the number of back-scattered gamma photons, and to filter out the X-rays.

Test experiments showed that the optimal geometry for the γ-γ coincidence method is when the detectors are at the closest to the sample (covering maximum solid angle). And the mass of the sample is chosen to cause no substantial pile-up (~10 000 count/second was ideal in the case of the detectors used). Theoretically the irradiating neutron flux can also be decreased by the use of smaller collimators, but this method was not applied, because it would require mechanical modifications on the apparatus.

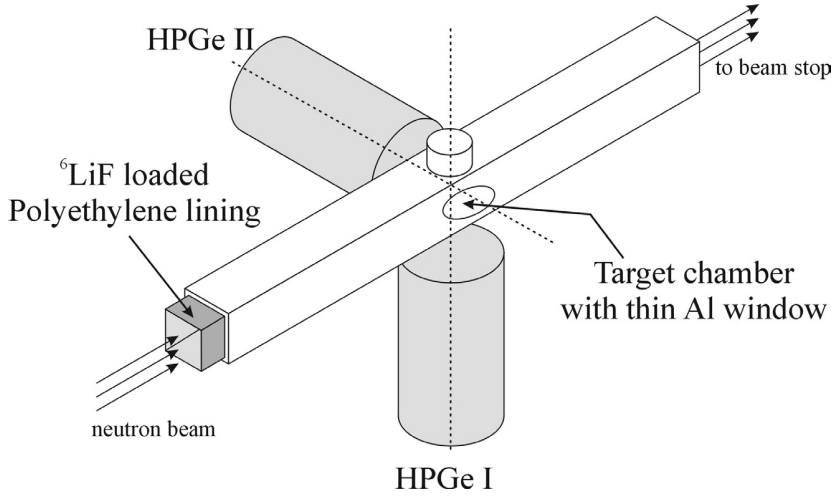

Figure 31 Detector placement for the standard setup [Ember 02a]

5.1.2. The coincidence electronics

The electronics used in the standard setup [Ember 02a] are shown in Figure 32.

The energy signals of the detectors were shaped and amplified by spectroscopy amplifiers. The amplifier signals were digitized with 16k analog-to-digital converters (ADC). The time signals of both detectors were connected into fast timing filter amplifiers. The amplified and shaped time signals were plugged into two constant fraction discriminators (CFD), which were used in ARC timing mode. The CFD signal of the detector HPGe–I started the time-to-amplitude converter (TAC). The CFD signal of the detector HPGe–II was delayed by

approximately 400 ns using a gate and delay generator, and it served as a STOP signal for the TAC. The TAC output of the time-to-amplitude converter was digitized with a homemade 4k ADC. The TAC single channel analyzer (SCA) logic output was connected into a level translator to be converted into one TTL and two NIM level signals. The TTL signal was used for gating the 4k ADC, which digitized the time spectrum. The NIM signals were fed into two segments of the gate and delay generator in order to synchronize them in time with the outputs of the spectroscopy amplifiers, and create the correct gating pulses for the two 16k ADCs that digitized the energy signals.

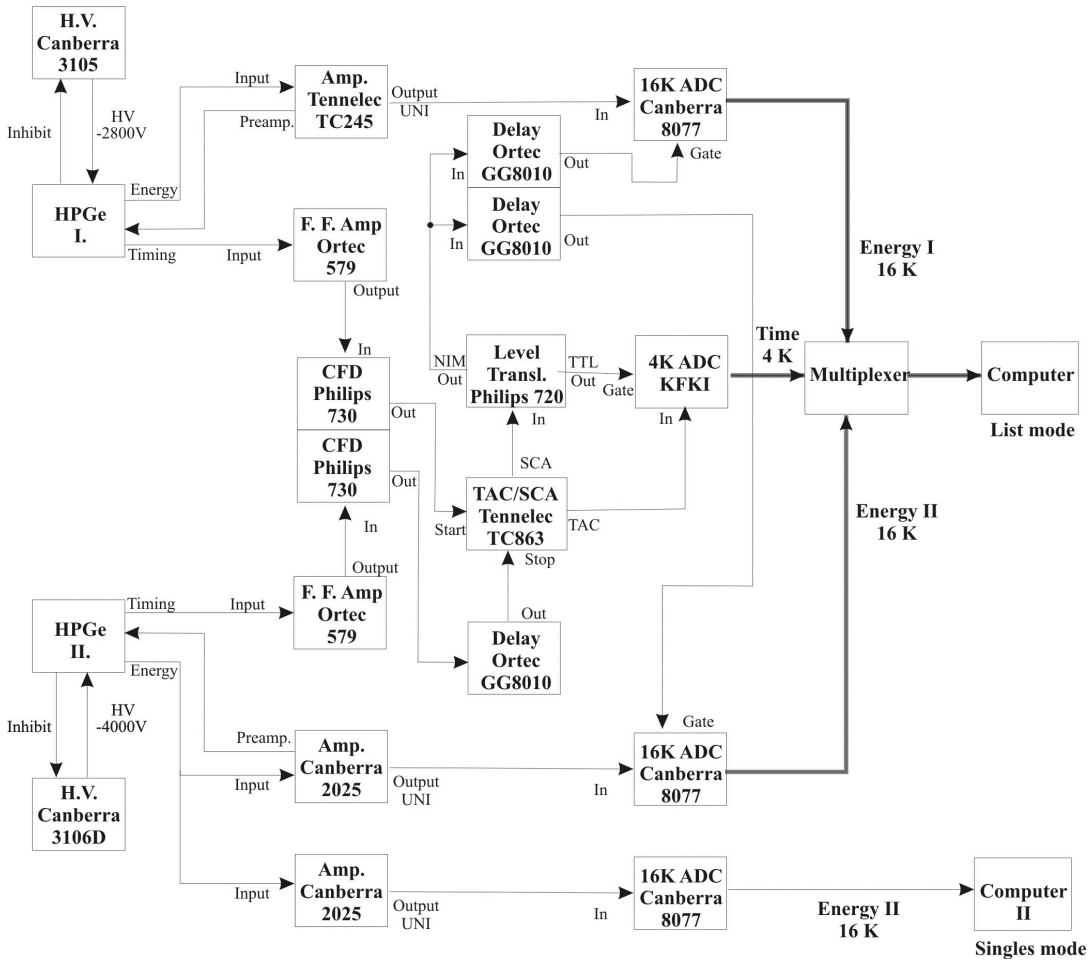

Figure 32 The γ-γ coincidence electronics for the standard setup[Ember 02a]

The energy signal of HPGe–II was also plugged into a fourth line (amplifier and ADC) without gating (not shown in Figure 32). An MCA board in a second computer collected this spectrum in singles mode. The formation of this fourth line had more purposes:

- Its spectrum was used as the neutron flux monitor of the system, At comparisons of elements of measurement series in the next chapters a certain peak of this spectrum was used for correction factor.
- It can serve as Singles spectra in comparisons.
- Coincidence detecting efficiency is relative to the product of two detector photo peak efficiencies, and as the detector photo peak efficiency decreases with energy, the coincidence becomes very inefficient at high energies (in our case it means E>2-3MeV, but the use of higher efficiency detectors would increase this energy limit), so the method is not practical above a certain energy. The low energy part of the singles mode spectra is very difficult to evaluate because of the Compton backgrounds and the spectral interferences of the numerous peaks. But its high energy part has efficiency good enough to obtain peaks with acceptable statistics, and it can be evaluated, because there are less peaks. So this forth channel might be used instead of the coincidence result at certain high energy peaks. This possibility was not used in the measurements in the next chapters.
- As it is an on-line measurement it can also be used for on-line monitoring if there is any mistake while measuring, like closed beam shouter or forgotten sample.

Approximately 400 ns of hardware delay was implemented on the timing signal of the detector HPGe–II. It causes 400 ns shift in the center of the time peak, without this delay the center of the time peak would be at t=0 , and only those events would be measured, where HPGe–I is fired first. But with this delay the system puts those events where HPGe-I was fired first after the center, and those events where HPGe-I was fired first before the center. E.g.: if HPGe-I was fired 20ns earlier than HPGe-II the event will be put to t=420ns, in reverse order the event will be put to t=380ns. See Figure 33.

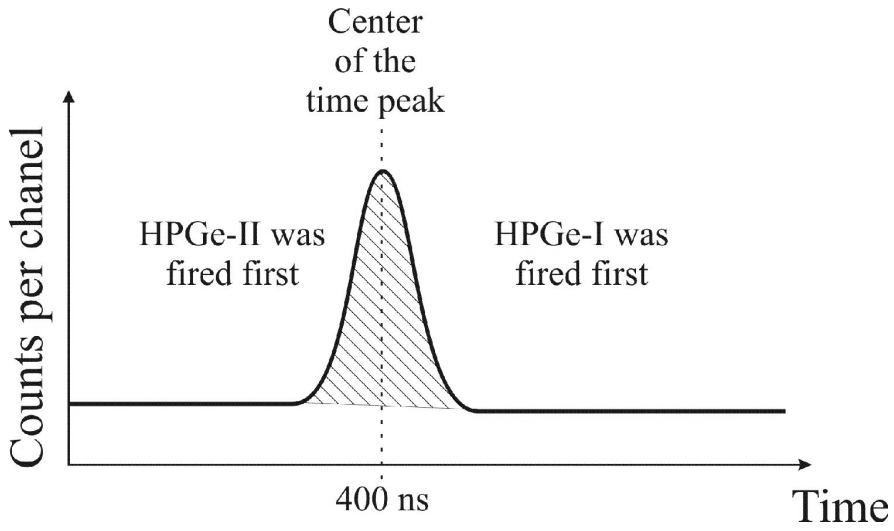

Figure 33 Effect of the hardware delay on HPGe-II

This 400 ns was chosen, because it is larger than the life time of any level of our interest (so it does not distort the coincidence), but is within the data collecting time of the Multiplexer (20 000 ns).

5.1.3. Data acquisition

The ADC data outputs were connected to a home-built multiplexer, which transferred the events to a PC-based data acquisition system [Héjja 97]. The multiplexer has 10 input channels compatible with the data output of CANBERRA ADCs. Its two outputs are connected to a PC with two I/O cards: a National Instruments 32-bit AT–DIO card for the list mode data acquisition, and a 64 k-word Multi Channel Analyser (MCA) board, which is a product of KFA Jülich. With a computer program the multiplexer can be configured via its XILINX logic chips through the AT–DIO board. The multiplexer is able to serve both the listmode and MCA mode data collections at the same time. The multiplexer data collecting time can be set in the range of 0-32768 ns for the list mode channels. It was 20 000 ns in the measurements detailed in this work. This time is the waiting time for the other ADC outputs to arrive after the first signal has arrived in any one channel. The collected data array is sent, after the waiting time has expired, to the AT–DIO card regardless of how many ADC outputs fired after the first one. Because of this, the list file can contain some data with no value. This is the so-called **independent** data collection mode. The name is given according that the effect can be caused by the independent thresholds of the timing and energy amplifiers. E.g.: if there is a time signal with no energy signal, that means that the signal was within the

thresholds of the timing amplifier, but out of the energy amplifier's. The independent mode is useful when double- and triple- or higher-fold events are to be collected at the same time.
The **dependent** mode is when no zeroes can be found in the list file. It can be obtained with veto signals obtained from data ready ADCs, or with software after the measurement. The gating on the ADCs in our standard setup highly reduces the number of empty signals, but the list file still contains some empty words (zeroes).

5.2. Data processing (peak to peak coincidence)

Figure 34 shows the workflow diagram of the data processing of a coincidence measurement (see Figure 30). One row of the list file makes up an event; **E1**is the energy measured by HPGe-I, **E2** is the energy measured by HPGe-II, **T** is the time passed between firing the two detectors. Thus the list file can be considered as a series of events.

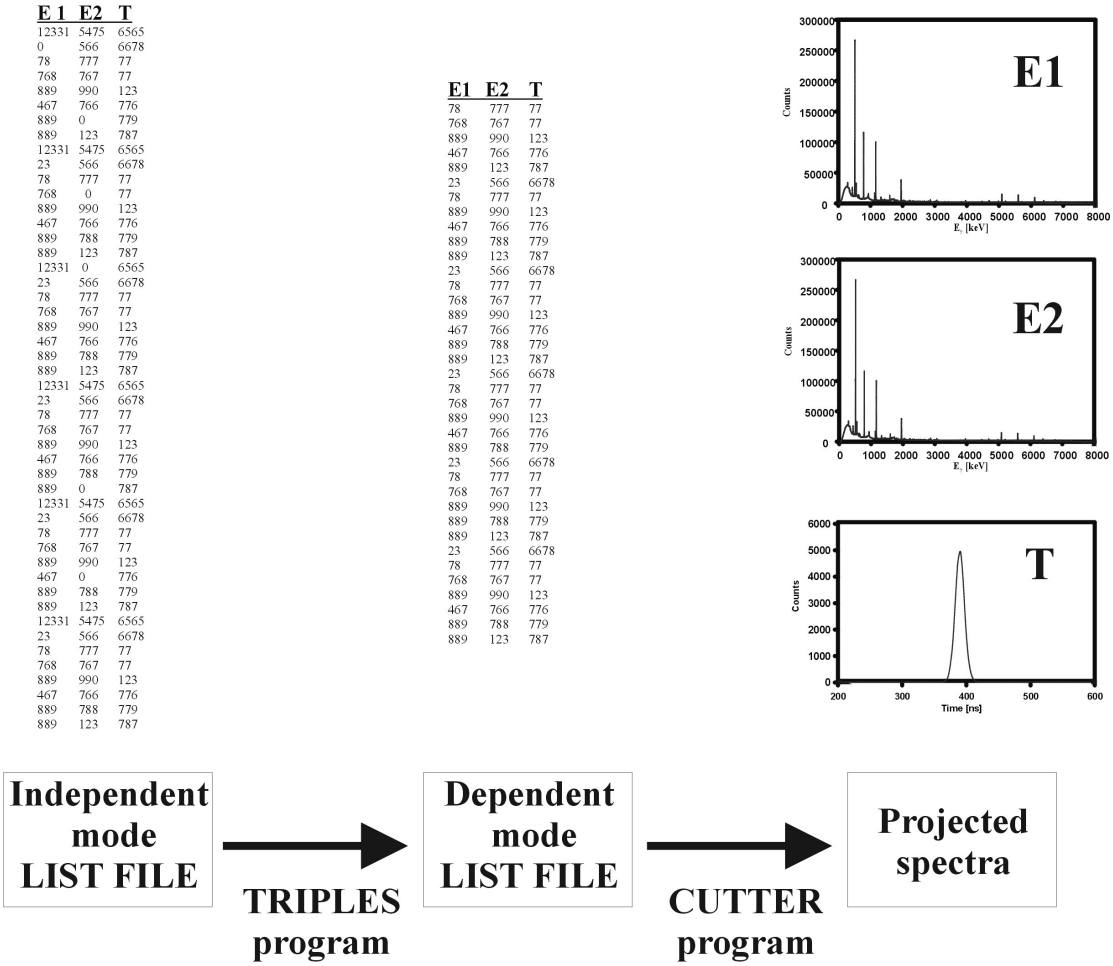

Figure 34 Data processing of a coincidence measurement

The list file collected by the multiplexer is considered as independent mode List file as it used to contain events where any of the numbers is 0.

The dependent mode, where signals from all the ADCs have to be present, is realized off-line after the measurement with a simple program (TRIPLES program) which removes all events

with any zeros from the list file. In the case of the standard setup, the gating of the ADCs highly decreases the number of records with empty words in the list file, but can not remove them completely. These are due to signals with amplitudes falling outside the range of one or more ADCs or the TAC.

The last step of data processing is the creation of spectra projections by applying software gates with the homemade program called CUTTER.

The original version of C++ programs TRIPLES and CUTTER were written by my supervisor Tamas Belgya, I improved these programs by adding additional features.

A projection means creating histogram(s) of a selection of events: the selection is made by setting certain conditions for the data ranges in some data columns. The simplest projection is the **total projection** which means creating three histograms of all values from the three columns of the list file. The total projection can be used to define conditions for other projections:

A **two-dimensional projection** is a projection where a gate is set only on one of the three columns. A part of a total projected energy spectrum is enlarged in Figure 35 to demonstrate the construction of a gate with background.

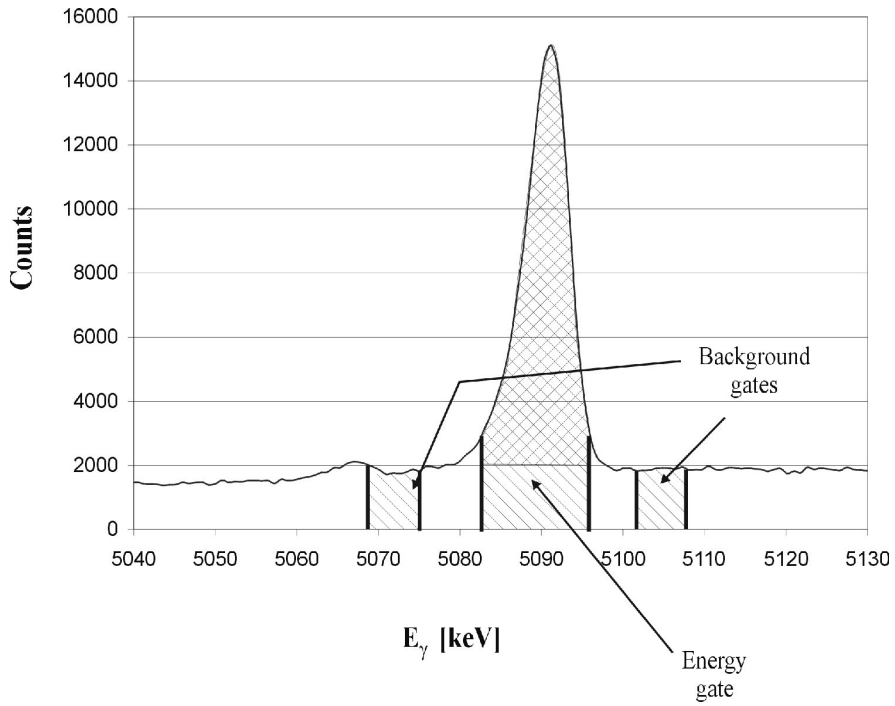

Figure 35 Gate settings example for a two dimensional projection

The peak area in the picture is marked as energy gate (G_e). This region contains real peak events (crosshatched in the picture), and background events (hatched in the picture) as well. It can not be determined if an individual event belongs to the peak or the background. If possible the background should be estimated from events on both sides of the peak. The two background regions combined cover the same number of channels as the peak gate and are noted as G_b. Assuming that the background events of G_e, and the events of G_b are from the same statistical sample, the projection of the background gate G_b represents the same number and behavior of events as the background part under the peak. Thus, the peak projection is estimated simply by subtracting the projection of G_b from the projection of G_e. This subtraction is made for each channel.

E.g.: using energy gate G_{E1} (from energy $E1_1$ to energy $E1_2$) defined on column E1 we keep only those events (rows) where $E1_1<E1<E1_2$ and create the E2 and T histogram (spectra) of these events. The cutting software also performs the background subtraction. This projection requires not only an energy gate, but a background gate G_b also. The background gate could be defined by taking some channels from before and some channels from after the peak (like on the figure). Separate E2 and T projections made on the energy and the background gate ($E2_E$,$E2_B$,T_E,T_B), then the background's histogram is subtracted from the energy's histogram channel by channel.

A **one dimensional projection** can be obtained if gates are set on two spectra.

Figure 36 illustrates the gate settings for one dimension projection. On the two axes the two gate settings are marked. The areas marked by I, II, III or IV mean groups of events from peak (P) or background (B) origin or both. The events from various origins can be selected in the following way. If Pi and Bi represent the events with peak or background origins in column I (e.g.: i=1 means column E1, and i=2 means column T) then the following projections can be created (in E2):

I: P1·P2 + P1·B2 + P2·B1 + B1·B2

II: P1·B2 + B1·B2

III: P2·B1 + B1·B2

IV: B1·B2

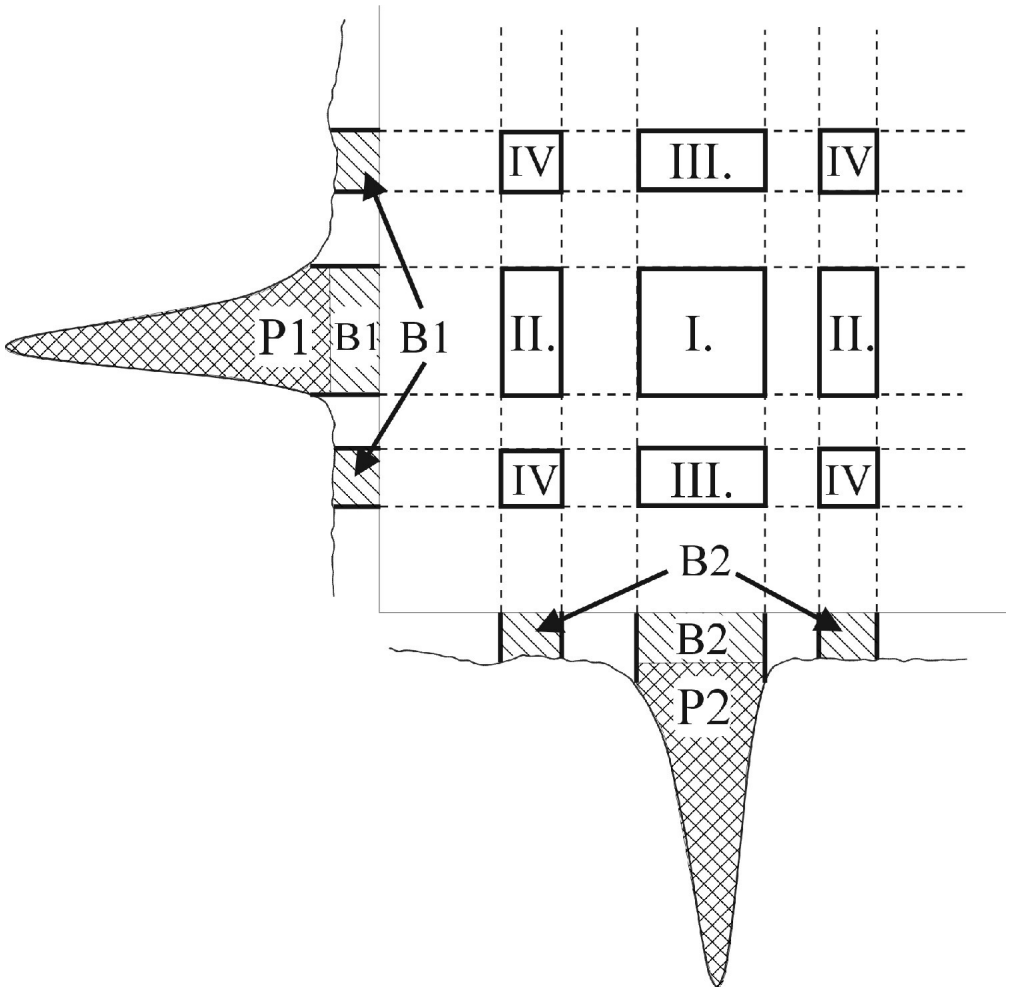

Figure 36 Schematic drawing of gate settings for a one dimensional projection

The formulas on the right sides mark the intersections of the drawing. E.g.: B1·B2 marks events of double background origin.

The real peak-peak coincidence events are marked P1·P2. It can be calculated from the above four sums as:

$$P1 \cdot P2 = \mathbf{I} - \mathbf{II} - \mathbf{III} + \mathbf{IV}$$

For any channel of the projected spectra this calculation is assumed to be true, thus in fact number **I, II, III, IV** can represent any channel of the corresponding spectra.

The above-described projections use the conventional peak-coincidence method, where the gates are set on one energy (E1) and the time (T) peak. This constraint reduces the spectrum

to the signals of those gamma photons in E2, which are in a cascade relation with the selected energy peak in E1. The method increases the peak to background ratio in E2, but also reduces the peak counts, since that is proportional to the product of two full energy peak efficiencies.

5.3. Coincidence measurement with ^{60}Co source

A measurement was performed with the standard setup with a ^{60}Co source of 7 kBq activity for 24 hours.

In this demonstration experiment, about 2% of the records in the list mode data files contained one or two blank words out of the three words making up a coincidence event. After using the triples program the dependent list file contained 9 million coincidence events.

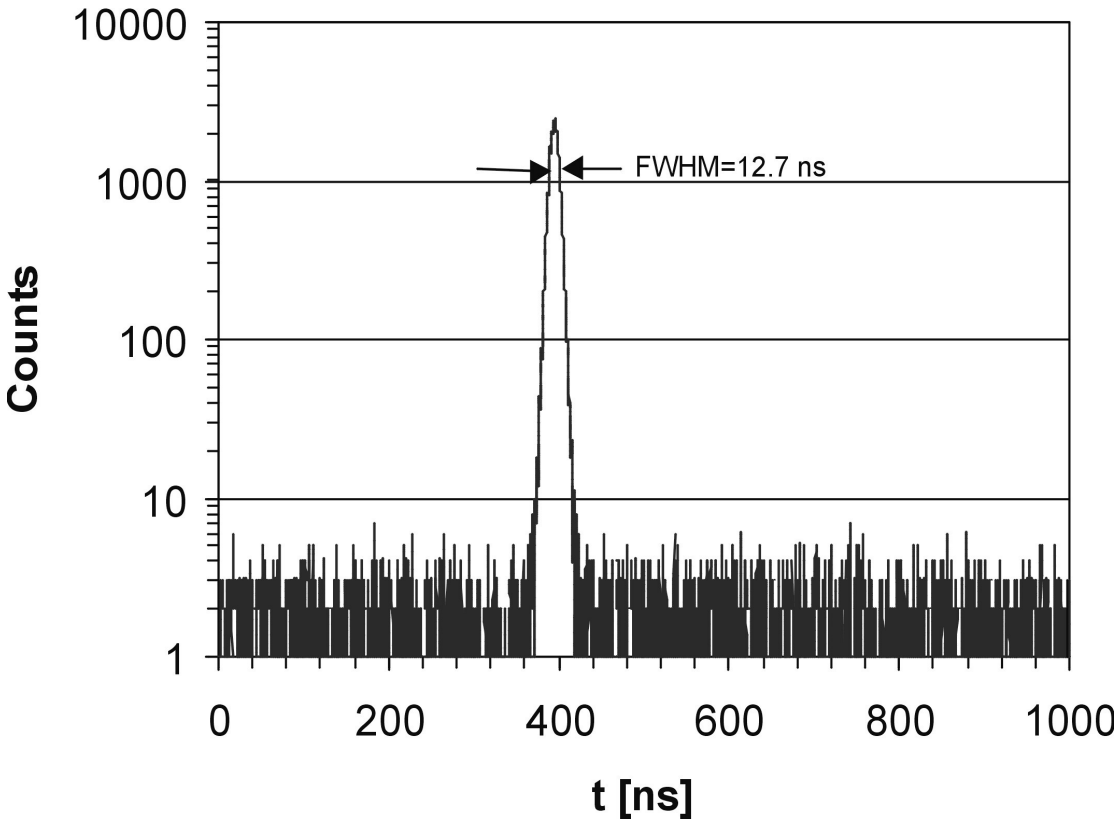

Figure 37 Time spectrum of ^{60}Co γ-γ coincidence events. Gates were set on the 1173 keV and 1332 keV γ peaks in the HPGe-I and HPGe-II energy spectra respectively [Ember 02a]

Figure 37 illustrates the time resolution of our system. Gates were set on the 1173 keV γ-ray peak in the energy spectrum of HPGe-I and on the 1332 keV γ-peak in the energy spectrum of the HPGe-II detector. The time resolution was found to be 12.7 ns full width at half maximum

(FWHM) as shown in the figure. The peak-to-background ratio was about 500 to 1. These values are valid for a single cascade (with narrow energy gates) only.

Figure 38 presents the total projection and the energy-gated cobalt spectra of the HPGe–I detector energy signals. Gates were set on the 1332 keV γ-peak in the HPGe-II spectrum, and on the time peak in the time spectrum. The ratio of the 1173 keV peak areas in the two cases was found to be 5.3. It is close to the total-to-peak ratio for the 1332 keV γ-peak (see Figure 43). The calculated suppression of the 1332 keV γ-peak relative to the 1173 keV γ-ray peak was 485 in the presented case.

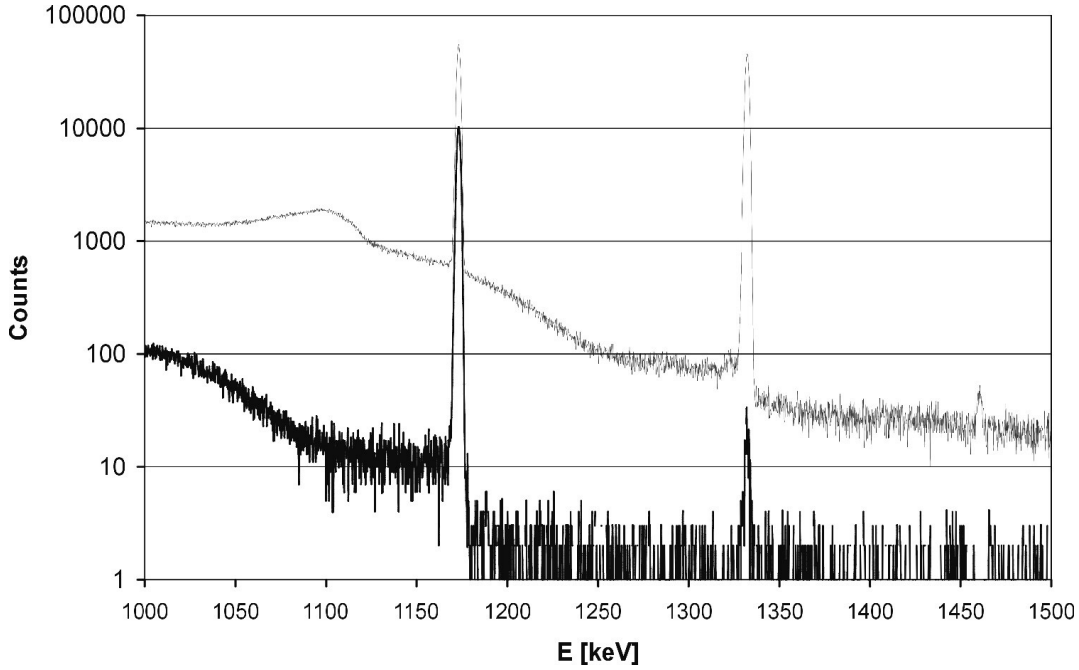

Figure 38 HPGe–I detector energy spectra. Thin line: total projection, thick line: gated with the 1332 keV γ-peak of the HPGe-II spectrum, and the time peak in the time spectra [Ember 02a].

5.4. Coincidence experiment with ^{35}Cl(n, γ) reactions

A sample containing chlorine was a PVC foil of 0.11 g mass and 1.8 x 2.5 cm^2 surface area. It was irradiated in our neutron beam and measured with the standard setup for 23 hours at the NIPS station. Most of the de-exciting γ-rays were from the ^{35}Cl(n,γ) ^{36}Cl reaction, due to its large cross section.

An amount of 48 million coincidence events were collected. The upper half of Figure 39 shows the total projected time spectrum. The time spectrum has a peak to background ratio of 150, and a FWHM of 30 nsec.

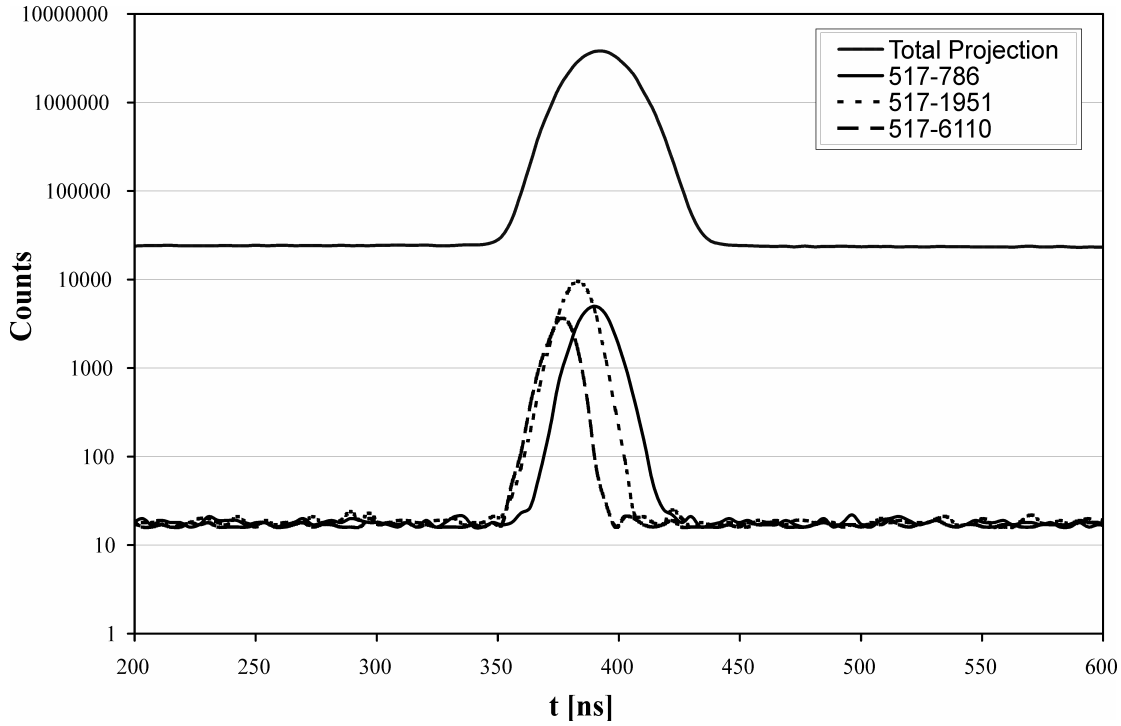

Figure 39 Total projection time spectrum from the ^{35}Cl(n, γ) coincidence measurement (upper), and time peaks for three peak-to-peak coincidences illustrating time walk [Ember 02b].

The structure of any time spectrum depends on many factors, such as detector parameters, threshold setting in the CFD electronics, and the various transition energies and life times of levels involved in the de-excitation process of the target nuclei. In the case of a broad energy range of transitions, one cannot obtain as good time resolution as can be obtained with e.g. the narrow energy gates of the ^{60}Co-calibration source. This is due to the time walk of the detectors [Knoll 00 - Chapter 17/IX]. In addition, finite lifetimes cause centroid shifts or

exponential tails, which also broaden the time peak. The lower half of Figure 39 illustrates the time walk by showing the time peak of three full energy peak-to-peak coincidences. In detector HPGe-I a gate on the 517 keV energy peak was set for all three cases, while in HPGe-II gates on the 6110 keV, 1951 keV and 786 keV peaks were applied respectively. The effect of the time walk is clearly visible; the time peaks of higher energy (higher amplitude) pulses are further from the center of the total projection time peak, while the lifetimes of the intermediate levels are negligible. The measured FWHM values for each of the three time peaks were about 13 ns, which is the same as was found for the ^{60}Co time peak.

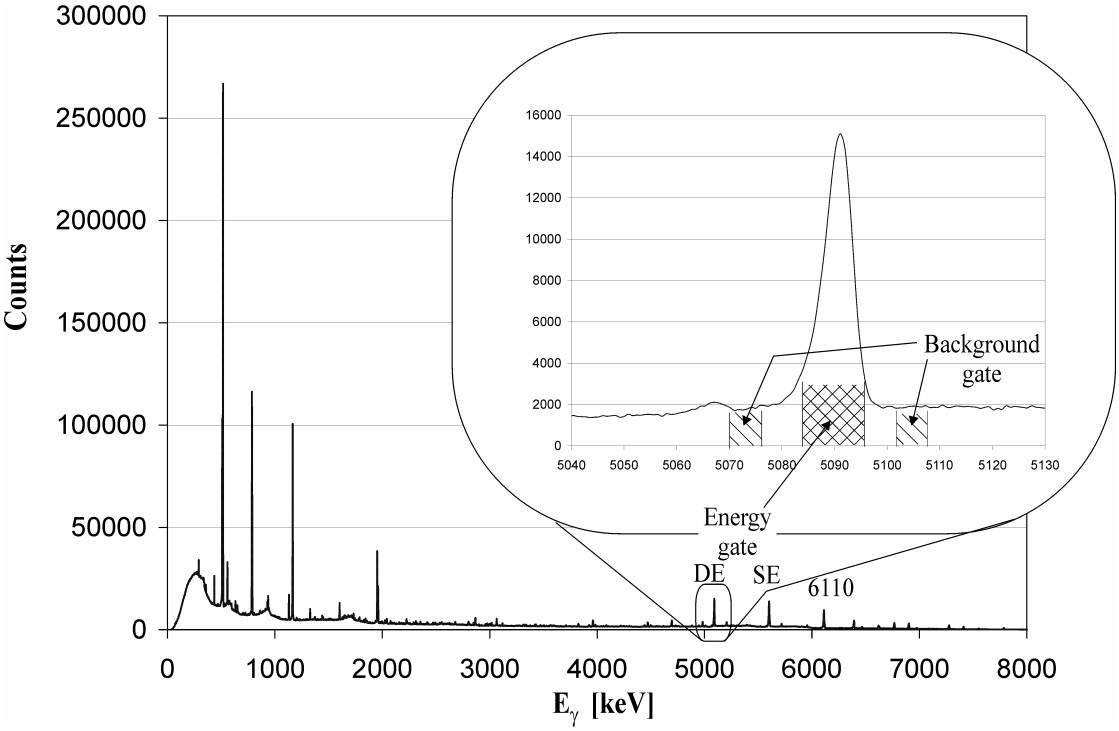

Figure 40 Total projection energy spectrum of the HPGe-I detector from the ^{35}Cl(n, γ) experiment [Ember 02b].

Figure 40 presents the total projection of the HPGe–I detector energy signals from the ^{35}Cl(n,γ) capture reaction. A few very strong lines dominate the spectrum, including the strongest primary transition of 6110 keV energy. To demonstrate the off-line coincidence analysis method, we set a gate on the 5086 keV double escape peak instead of the 6110 keV full energy peak, because the latter and its single escape peak form doublets with the single– and double–escape peaks of a weaker, higher energy γ ray. The peak and background gate settings are shown as gridded and cross-hatched areas, respectively, in Figure 40.

In Figure 41 the spectrum of the γ-rays measured by the HPGe–II detector with the gate settings explained above is shown. The strongest coincidence peaks are labeled with their energies. The signal to noise ratio is very good. The random coincidences have almost completely disappeared, as illustrated by the magnified insert of the energy-gate setting area.

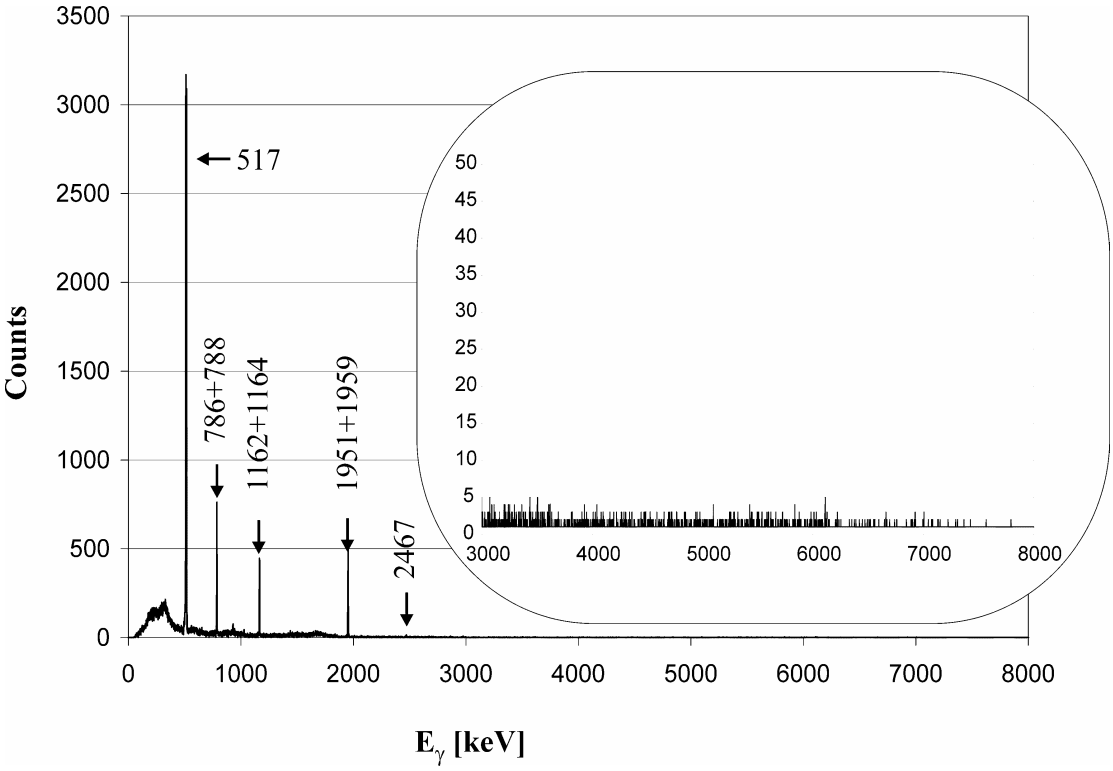

Figure 41 Spectrum of γ-rays in coincidence with 5086 keV, the double escape peak for 6110 keV γ-ray.

Figure 42 shows the corresponding decay scheme [TOF 99] for the $^{35}Cl(n,\gamma)^{36}Cl$ reaction, retaining only those transitions which are expected to be in coincidence with the strongest 6110 keV primary capture γ–ray. For easier reading the γ-ray energies and their absolute intensities in percentage are rounded off. The γ transitions with intensity less than 1% are drawn with dotted lines.

In agreement with our expectations, the gated energy spectrum of HPGe-II contains only the peaks expected from the known level scheme of ^{36}Cl. The weak 2467 keV line can be easily identified, but the similarly weak 508 keV line is masked by the 511 keV annihilation peak.

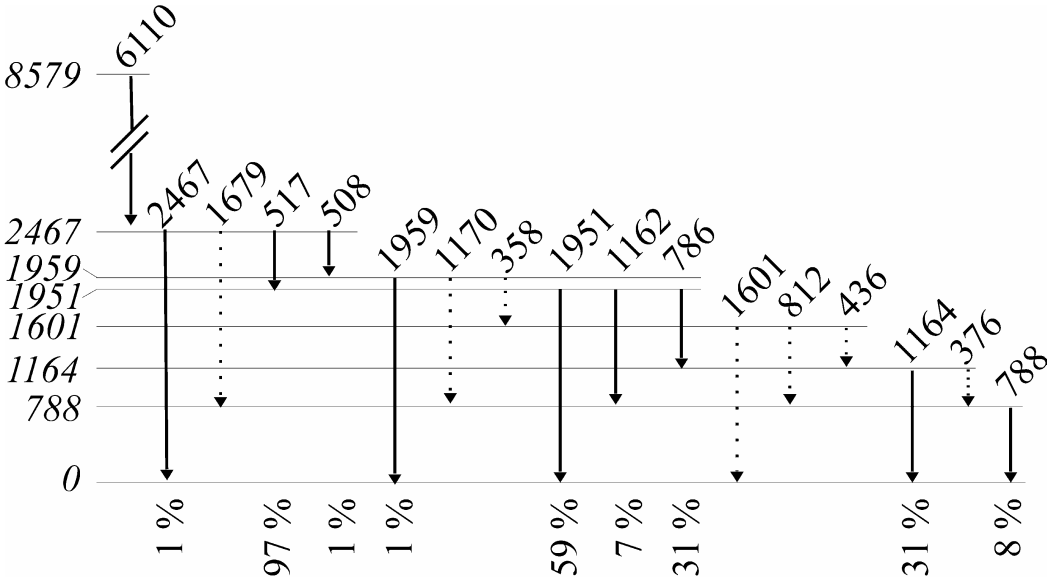

Figure 42 Partial decay scheme of ^{36}Cl. Only the lines in coincidence with the 6110 keV peak are shown [TOF 99].

5.5. Total to peak ratio

A commonly used method to determine the total to peak ratio is to measure the gamma spectra of single line sources. The total to peak ratio for the energy of that peak can be calculated by dividing the total number of detectable events (peak and its continuous Compton background together) and the events in the full energy peak as described in Chapter 3.6.

The number of available single line sources is limited (under ten), also their energy range is too small compared with the energy range required by PGAA (100 keV-11MeV).

The single line data set can be extended with the PGAA sources having single line prompt gamma transition. For example, the single line PGAA spectrum of hydrogen is shown in Figure 17.

The total to peak ratio was determined for the "*γ-ray detector #1"* (see Table 13) of the NIPS facility with the method described above. A linear polynomial was found to be a satisfactory fit to the data. The result is shown in Figure 43.

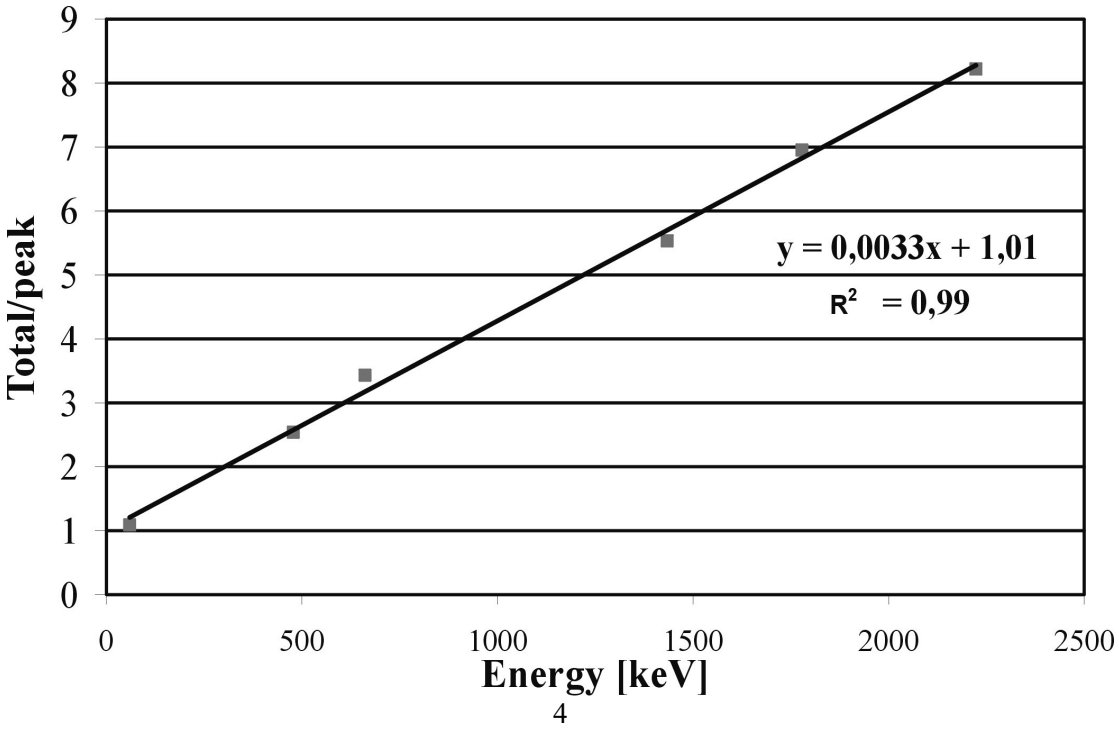

Figure 43 Total to peak ratio as the function of gamma energy

Table 4 shows the data of the figure, the source isotope, its energy, and the peak to total ratio calculated.

Table 4 Gamma lines of isotopes used for the total to peak ratio

Element	γ energy [MeV]	Total to peak
Am-241	59,5	1,10
B	478	2,60
Cs-137	661,6	3,26
V	1434	6,03
Al	1778,7	7,27
H	2223,23	8,86

The energy function of the total to peak ratio in Figure 43 shows that the higher the gamma energy, the larger part of the events is detected in the continuous background rather than in the peak. Thus peak to peak coincidence is not effective. A method that can use some of the events from the continuous background could increase the effectiveness of the coincidence method substantially and is discussed in the next section.

5.6. The γ-γ regional coincidence method

As we have seen in the previous section, large part of the events detected by the HPGe detector is in the continuous background rather than in the photo peak. To improve the coincidence efficiency I elaborated the so called γ-γ regional coincidence method [Ember 02]. In the γ-γ regional coincidence method a gate is set on a part of the spectrum which includes one or more peaks and a part of their Compton continuum instead of a single peak (like in peak to peak coincidence). Peak to peak coincidence is a special case of regional coincidence.

5.6.1. Choosing the optimal region for the gate

Optimum gate for a selected peak is the gate of the projection which makes the best peak statistics. It can be found by comparing the results of projections with different regional gates on the spectrum. Steps to be done:

–Select gates to be compared

Using the decay scheme of the isotope I make a list of the most intense peaks in coincidence with the selected peak, and the matrix peaks. Usually I define the possible gate regions by starting with the highest energy peak, and set the first regions upper limit to include it, and the lower limit just above the second highest energy peak in the list. The next region involves this second peak also. If the distance is big between two peaks, it is also possible to go by e.g. 1000 channel steps.

–Compare the results

Due to the number of possibilities to be compared usually I do not evaluate the spectra of all projections to obtain exact statistical values. Instead make a simple pre-selection. First I observe the peak shapes, and keep only those projections where the peak shapes looks Gaussian with the less interferences. Then I evaluate their projected spectra, and select the one with the best peak to background ratio or with the best peak uncertainty. In most cases there are more selections with acceptable statistics. I mark them, and after checking more peaks, I select one that is acceptable for other peaks of interest also.

The following example will make it easier to understand:

Example:

For this example the dataset of the measurement in chapter 5.7 is used. All details of the measurement and the samples can be found there. Here I use the data only to show an

example of finding the optimal gate conditions for a selected peak. I select the Chlorine peak at 517 keV. As can be seen on Figure 42 this peak has the following coincidence lines: 6110, 1951, 1162-1164, 786-788. Note: I do not differentiate the doublets. I also put the 2223 keV line of Hydrogen into this list. Also I make projections between 6110 and 2223 with 1000 channel steps. Table 5 shows the gates set for the projections. Projection "*p2p"* is the peak to peak coincidence, and projection "*total"* is the total projection.

Table 5 Gate settings for the example

number of projection	E min	E max	Description
p2p	6103	6120	Peak to peak
p-2	5500	6120	
p-3	4850	6120	
p-4	4200	6120	
p-5	3550	6120	
p-6	2900	6120	
p-7	2250	6120	
p-8	1960	6120	with Hydrogen peak
p-9	1180	6120	with peak 1951
p-10	800	6120	with peaks 1162-1164
p-11	525	6120	with peaks 786-788
total	0	Max	total coincidence

Figure 44 show the projected spectra magnified around the peak of interest.

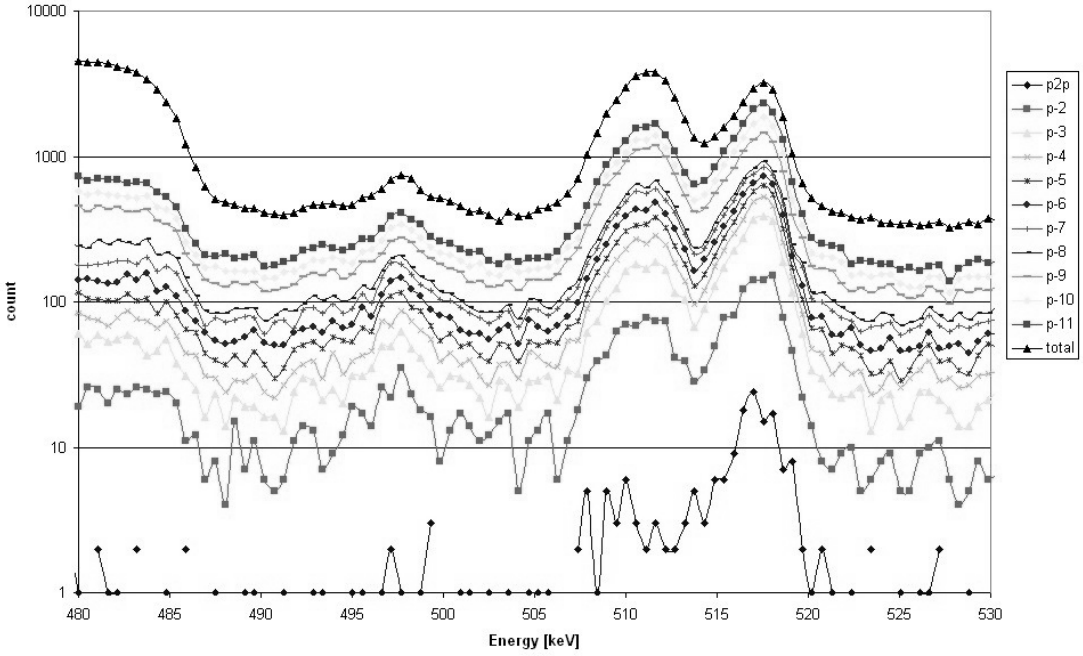

Figure 44 Spectra of the projections around the selected peak

For better overview I connected the points of the spectra on the figure. As can be seen the peak to peak coincidence gave a peak 2 order of magnitudes smaller than the total projection. Although its background is (almost) zero, and the 511keV peak is very small. Table 6 contains the peak statistics evaluated with the program Hipermet-PC. The last column contains my first selection conditions: beak area/(average background* full width at half maximum).

Table 6 Peak statistics for the different gate settings

number of projection	Peak Area	FWHM [keV/chnl]	Average background	Peak/ bkg
p2p	106±11.3%	2.88/5.37	1.4 ±21.4%	14.10
p-2	852±4.7%	3.26/6.00	11.9 ±12.6%	11.93
p-3	2156±3.6%	3.26/6.00	26.4 ±9.8%	13.61
p-4	2774±3.1%	2.96/5.53	35.4 ±8.2%	14.17
p-5	3362±3.2%	2.98/5.57	47.9 ±8.4%	12.60
p-6	3848±2.7%	2.99/5.58	63.4 ±7.3%	10.88
p-7	4487±2.7%	3.06/5.71	78.9 ±8.0%	9.96
p-8	4801±2.4%	3.04/5.67	88.3 ±6.7%	9.59
p-9	7551±2.3%	3.08/5.74	132.9 ±5.0%	9.90
p-10	9699±2.4%	3.03/5.6	177.3 ±4.7%	9.77
p-11	12182±2.2%	3.05/5.7	208.4 ±3.8%	10.26
total	16765±2.5%	3.05/5.7	383.9 ±4.9%	7.66

According to Table 6 projections p-4 or p-11 are the best choices for peak 517 keV. In this case peak to peak coincidence is not practical due to the low count and high statistical uncertainty of the peak. Any regional coincidence gives better statistics. It is also clear, that any one of the regional coincidence gates could be chosen. It means gate selection is not critical for the 517 keV line, so it requires no separate projection, it can be evaluated from a projection optimal for other peaks. E. g.: in chapter 5.7 gate of projection p-7 was selected, because that gate was close to optimal for more peaks.

5.6.2. Properties of the regional coincidence method

The regional coincidence method gives a higher peak count, but also gives higher background ratio than peak to peak coincidence. Higher peak count usually results in lower peak uncertainty, but in some cases the unwanted spectral interferences remain, hardening the peak evaluation. This is why the regional coincidence method requires the time consuming optimal gate search. In the case of a measurement series, the optimal gate search is even longer.

When using standard based relative method for the calculation of the concentrations, separate optimal gates can be defined for groups of peaks, or even for every separate peak, but in most cases it is possible to find one gate setting close to optimal for almost all peaks in interest.

In the case of γ-γ regional coincidence method the background subtraction is made only for the time peak. No background gate could be set for energy gates. Experience shows it is enough.

5.7. Comparison of the PGAA γ–γ regional coincidence method with the Compton suppressed spectrometry

The same sample has been studied under three different experimental arrangements: the Compton suppressed spectroscopy, the traditional singles mode and the γ-γ regional coincidence method. These measurements were made in 2000 prior to the construction of the NIPS facility, so all measurements took place at the Compton suppressed spectrometer facility. The experience gained in these measurements helped the construction of the NIPS facility. For all three cases the neutron beam was collimated to approximately 2 cm by 2 cm with an essentially constant incoming neutron flux of $2*10^6$ $cm^{-2}s^{-1}$. The HPGe detector of the Compton suppressed spectrometer was used in all three setups, this fact is important for their comparison. The parameters of the detector can be seen in Table 11 in the appendix. Each individual measurement was performed for 13700 s (live time) for comparison.

The Compton suppressed spectrometer is described in Chapter 4.3.
In the singles mode experiments, the HPGe detector with no BGO annulus was placed 2 cm from the sample. With this setup we could maximise the solid angle while still maintaining some passive shielding. The electronics of the Compton suppressed spectrometer were used for the accumulation of the singles mode spectra.
The third arrangement was a coincidence setup similar to the one described in Chapter 5.1, but with the HPGe detector of the Compton suppressed spectrometer and the "*detector #1*" from Table 13 in the appendix. The two detectors were placed opposite to each other (Position I and II in Figure 28) and perpendicular to the neutron beam. Both detectors were positioned at 2 cm from the centre of the sample. A 2 mm layer of ^{6}LiF loaded polyethylene protected both detectors from scattered neutrons. A 1 mm thick lead plate was used to cut down the number of X rays, back-scattered and other low-energy gamma photons, which would only increase the dead time of the electronics. The γ-ray energy signals were digitalised in 16K channels and the time signal in 4K.
Due to the size of the target chamber the closest detector position could have been 4.5 cm from the centre of the sample, so to achieve a closer geometry, the target chamber was removed in the last two setups.

For these experiments a test sample was prepared. The ingredients were chosen to simulate a certain matrix effect (described in Chapter 4.4). Solutions of $CoCl_2$ and H_3BO_3 were chosen. The sample contained two of the most problematic matrix elements for PGAA: hydrogen and boron. As noted in the introduction, the main problem with this sample is the high Compton background due to the γ rays of boron and hydrogen. All the intense cobalt lines and some of the low-energy chlorine peaks are situated on this background. Moreover, the back-scattering peak of hydrogen also interferes with the most intense peak of cobalt at 229 keV.
The sample contained 1 ml solution in a sealed teflon container. The mass concentrations of the ingredient elements are shown in Table 7 in mass percent. The last row of the table gives the total sample mass in mg.

Table 7 Composition of the solution, and total mass of the sample

Element	Sample concentration [m%]
H	11.0
B	0.37
Cl	0.28
Co	0.23
O	88.13
Total mass [mg]	1000.0

The spectra of the sample accumulated in the three different setups are shown in Figure 45. For easier comparison of the shapes of the three spectra, the counts of the ungated singles spectrum were divided by 9; thus the height of the hydrogen peak became the same as in the Compton-suppressed spectrum. The third spectrum in the figure is a regional coincidence spectrum, created by defining a coincidence relation with every event having energy higher than 2230 keV (just above the hydrogen peak).

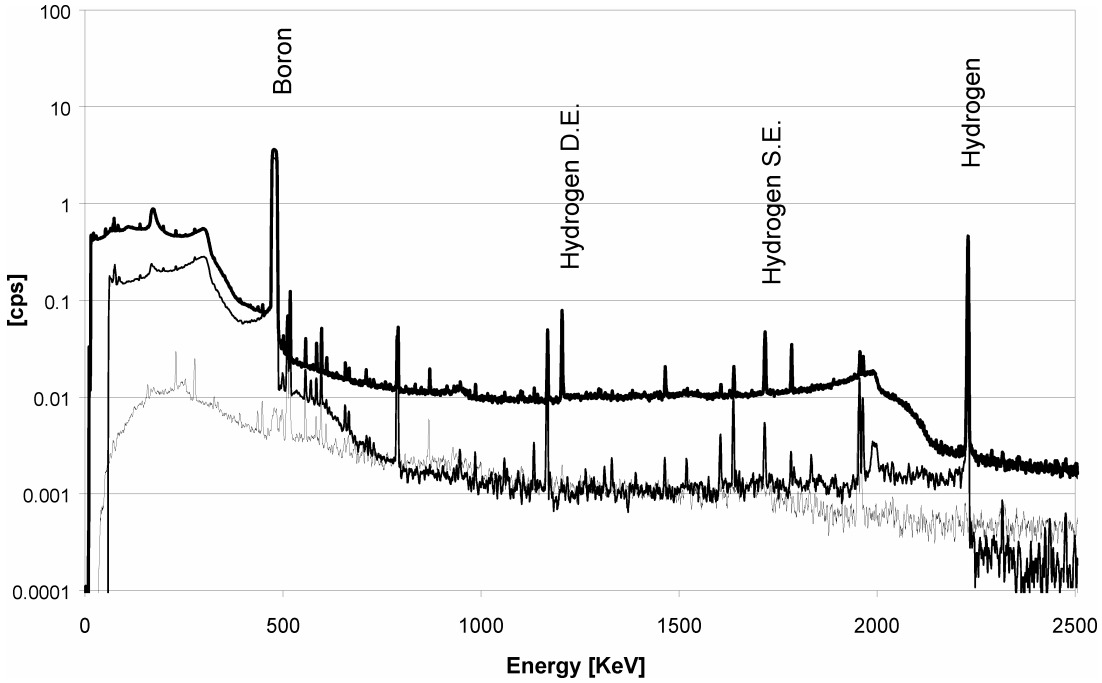

Figure 45 Spectra of the test sample. Thick line: ungated singles/9, medium-thick line: Compton suppressed, thin line: coincidence [Ember 02].

In Figure 46 the low energy parts (under 550 keV) of the same spectra are enlarged.

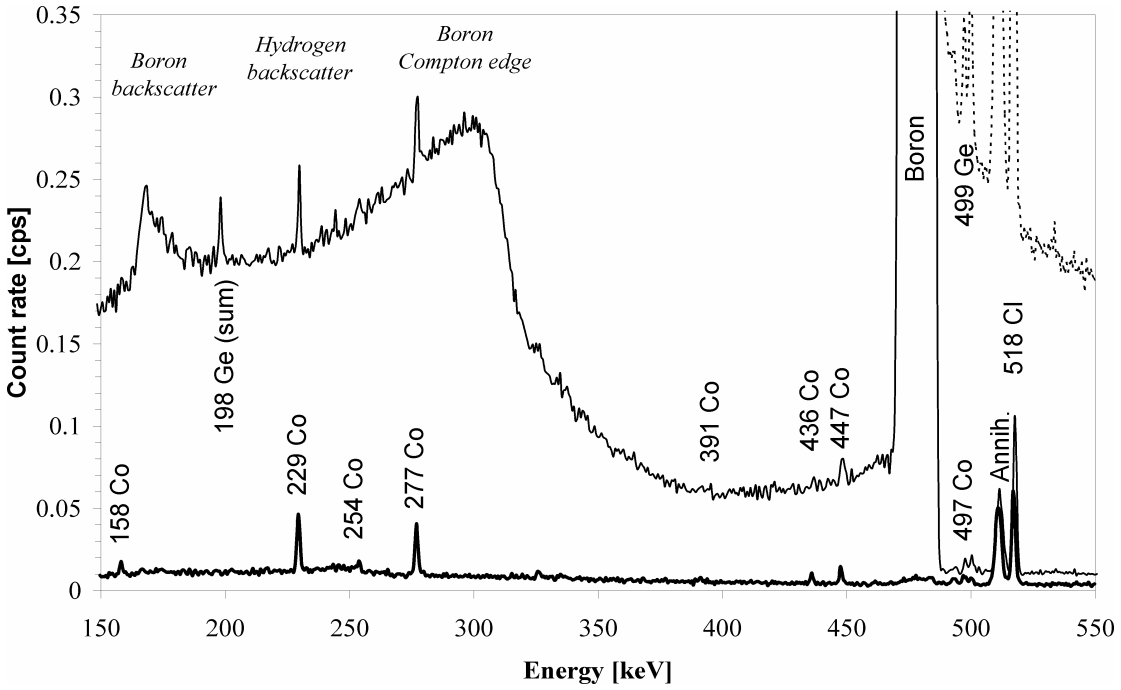

Figure 46 Spectra of the test sample. Dashed line: ungated singles/9, thin line: Compton suppressed, thick line: coincidence [Ember 02].

Comparing the singles and the Compton-suppressed spectra, we can make the following observations:

1. The Compton suppression reduces the hydrogen single-escape peak to full-energy peak ratio by a factor of 10, and reduces the double-escape peak to unidentifiable.
2. The detector was at 23.5 cm from the sample in the Compton-suppressed case but only at 2 cm in the singles case. Due to the longer distance from the sample, the hydrogen peak is lowered by a factor of 9.
3. Furthermore, the continuous Compton background is lowered by a factor of ~100 at γ-ray energies between 1 and 2 MeV. However, the boron peak and its Compton background still dominate the low-energy part of the spectrum. Peaks below the boron peak can hardly be seen against this background. The Compton background due to boron is reduced only by a factor of 20-40, showing that the Compton suppression is very energy dependent, and is less effective at low energies.

In comparison, the coincidence method highly simplifies the spectra by completely removing the hydrogen peak, its Compton edge, and both of its escape peaks. The boron peak and its Compton continuum are also reduced substantially, making the low-energy γ rays much more visible. Figure 46 also shows that the cobalt peak at 158 keV can be identified only in the coincidence spectrum, whereas the background peak at 198 keV has been eliminated completely.

Table 8 Signal to noise ratio (=total peak area/average background) for the three setups with sample S1. Total peak areas and average backgrounds/channel are also given.

	Singles mode			Compton suppression			Coincidence		
E [keV]	peak [cps]	bkg [cps/ch]	S/N	peak [cps]	bkg [cps/ch]	S/N	peak [cps]	bkg [cps/ch]	S/N
229	1.39	4.21	0.33	0.09	0.20	0.46	0.089	0.011	7.78
277	0.96	4.26	0.22	0.10	0.26	0.39	0.079	0.0093	8.48
518	2.38	0.26	9.15	0.23	0.01	23.27	0.16	0.0048	32.69
1164	1.32	0.09	15.27	0.17	0.001	155.35	0.10	0.0015	75.58

Table 8 shows the total peak areas and their average background counts (for one channel) in cps for the two most intense cobalt peaks (229 keV, 277 keV) and two intense chlorine peaks (518 keV, 1164 keV). The table also shows the signal/noise ratio calculated by dividing the peak area with the average background. The Compton suppression gives a 1,5-2 times better peak-to-background ratio than the ungated singles, while the γ-γ coincidence method gives a

25-40 times better value at low energies. With the present conditions the signal/noise ratio for the highest energy (1164 keV) is best with the Compton suppression. For high energy γ rays (above 2 MeV) the singles mode has the best signal/noise ratio.

The effect of the region selection is also interesting. Figure 47 shows the Compton suppressed spectra with 3 different projection settings: the total projection, the E>520keV, and the E>2230keV (this is the one presented on Figure 45 and Figure 46)

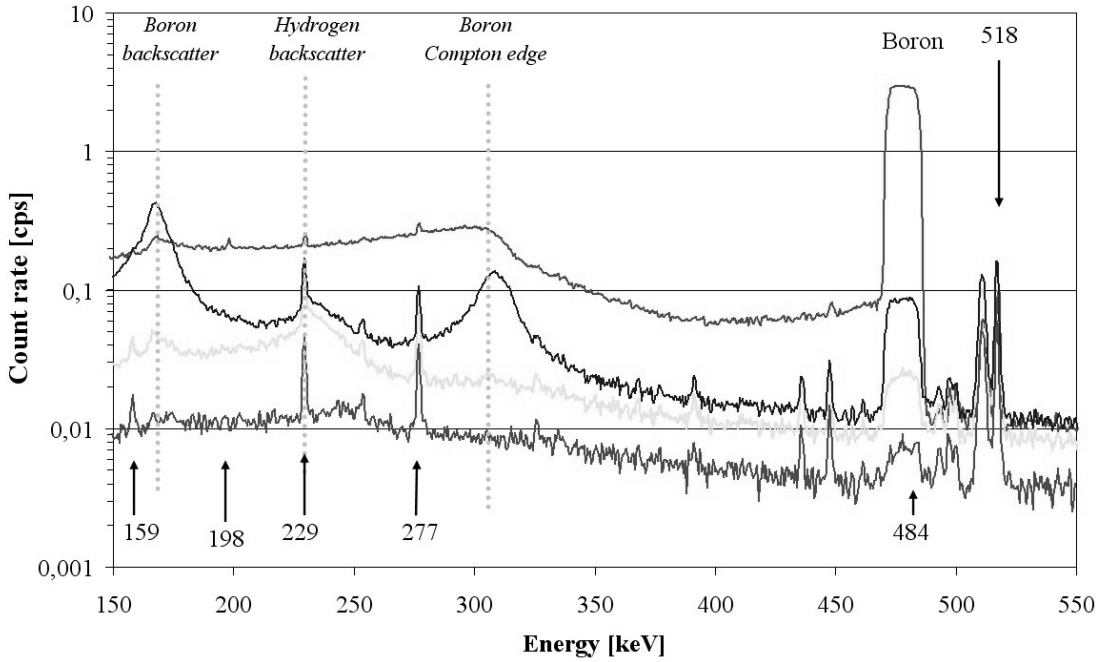

Figure 47 Effect of the different region selections spectra from up to down: Compton suppressed, total projection, region 520 keV+ , region 2230 keV+

The Total projection suffered the backscatter of boron, that was eliminated in the E>520keV projection, where the Hydrogen backscatter was still problematic. This is why E>2230keV was chosen as regional coincidence gate.

This measurement gave us important information for the design of the NIPS facility:

- Showed, that the coincidence method can compete with the Compton suppression,
- After testing different geometries, it became obvious, that the closest geometry is the best.
- The big backscatter required the creation of an alternative detector position bellow the guide to be able to use two detectors perpendicular, which geometry decreases this effect.

5.8. A series of measurements with cobalt chloride in boric acid solution for the calibration of the coincidence method

As a sequence to the measurement in Chapter 5.7, four similar samples with different concentrations have been studied using the γ-γ regional coincidence method. These measurements were also made in 2000 prior to the construction of the NIPS facility, so to assure the reproducibility of measurement geometry, all measurements took place in the target chamber of the Compton suppressed spectrometer. The neutron beam was collimated to approximately 2 cm by 2 cm with an essentially constant incoming neutron flux of $2*10^6$ $cm^{-2}s^{-1}$. The HPGe detector of the Compton suppressed spectrometer (parameters can be found in Table 11) and "*detector #1*" from Table 13 in the appendix was used. The detectors were positioned opposite to each other (Position I and II in Figure 28) and perpendicular to the neutron beam. Each individual measurement was performed for 13700 s (live time) for easier comparison. Due to the size of the target chamber, both detectors were positioned at 4.5 cm from the centre of the sample. A 2 mm layer of ^{6}LiF loaded polyethylene protected both detectors from scattered neutrons. A 1 mm thick lead plate was used to cut down the number of X rays, back-scattered and other low-energy gamma photons, which would only increase the dead time of the electronics. The γ-ray energy signals and the time signal were digitalised in 16 K channels, and in 4 K channels respectively.

For these experiments solutions of $CoCl_2$ and H_3BO_3 with four different concentrations were prepared in sealed teflon containers. All samples (S1, S2, S3, S4) contained boron and hydrogen with approximately the same concentration. The concentrations are shown in Table 9 in mass percent for each sample. The last row of the table gives the total sample mass in mg.

Table 9 Composition of the solutions, and total masses of the samples

Element	Sample concentration [m%]			
	S1	S2	S3	S4
H	11.55	11.77	11.68	11.98
B	0.39	0.41	0.40	0.42
Cl	0.65	0.36	0.10	0.02
Co	0.54	0.30	0.08	0.01
O	86.85	87.16	87.74	87.56
Total mass [mg]	2544.7	2337.8	2749.9	2463.6

The samples were accurately positioned in the target chamber to assure the reproducibility of measurement geometry. Because of this geometric precision these four measurements were

adequate for the determination of the count rate as a function of concentration (calibration curve). To obtain the calibration curve, a correction was applied to the neutron flux variations: The hydrogen peaks from the spectra collected in singles mode with the second detector were used as a neutron flux monitor. The peak areas in the coincidence spectra were multiplied by the ratio of the corresponding hydrogen peaks, setting the correction to unity for S1.

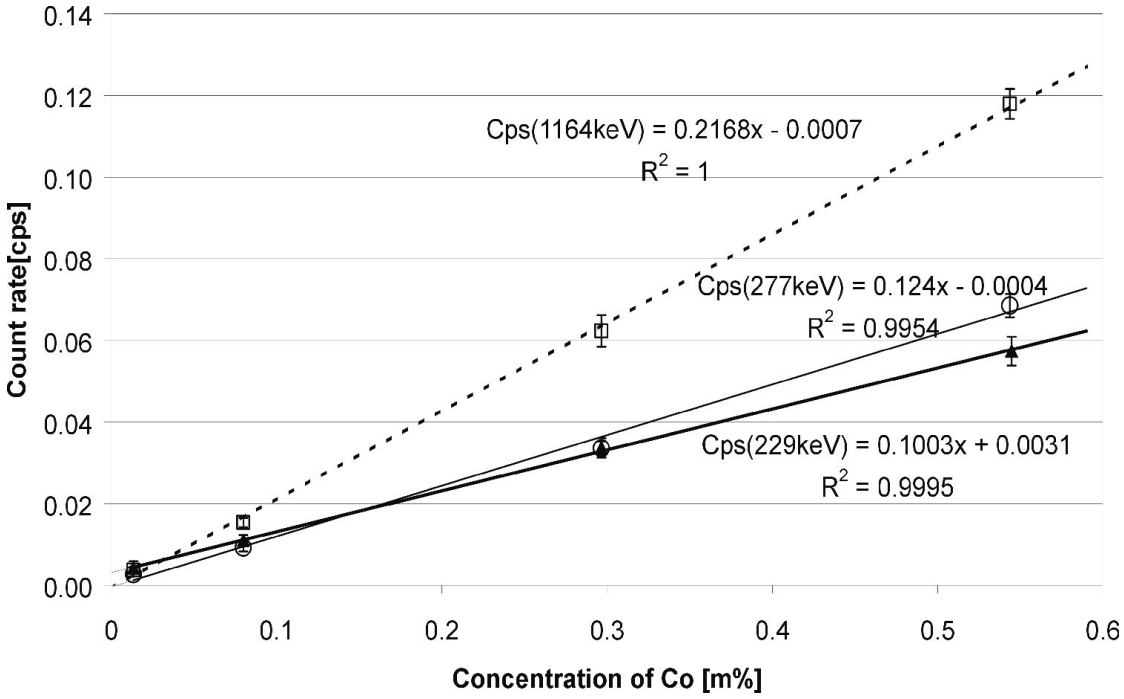

Figure 48 Calibration curve for the 229 keV (thick line), 277 keV (thin line) cobalt peaks, and 1164 keV (dashed line) chlorine peak [Ember 02].

Figure 48 shows the calibration curve for the two most intense peaks of cobalt at 229 keV and 277 keV (solid curves), and for a chlorine doublet at 1164 keV (dashed curve) for comparison. As can be seen in the figure, the count rates increase linearly with concentration. The calibration curves for the 277 keV and the 1164 keV peaks go (within the 1σ uncertainty) through the origin, but the 229 keV calibration curve is only within 3σ of the origin. This is because, as described earlier, the maximum of the hydrogen back-scatter peak is just under the 229 keV Co peak. Back-scattering gives a true coincidence between the two detectors, and the lead shielding layers could not eliminate it completely. Change in the geometric positions of the detectors might be a help in this problem. For instance, placing the detectors

perpendicular to each other (and the neutron beam), instead of opposite to each other should reduce the number of back-scattered events.

This measurement also gave us important information for the design of the NIPS facility:

- The problem caused by the backscatter strengthened the need of an alternative detector position bellow the guide to be able to use two detectors perpendicular, which geometry decreases this effect.

5.9. Application: Inactive tracing of glass melting furnaces with coincidence

This was a practical industrial application for coincidence PGAA. The problem was originally solved with the Compton suppressed spectrometer in 1998. The problem and the original measurement is detailed in Chapter 4.4.

The goal of the re-measurement was to see whether the problem can be solved better with the coincidence method.

5.9.1. Samples and sample preparation

Four were taken from the borosilicate glass samples described in Chapter 4.4. The original samples measured with the Compton suppressed spectrometer weighed around 50 grams, but they did not fit into the NIPS target chamber, thus pieces of about a half-gram was cut from each for the purpose of coincidence measurements.

As the 50 grams samples are very small benchmarked to the amount of glass they were taken from, it may be hypothesized, that they are homogeneous. But to decrease the chance of measuring an incomparable part of them, more little splinters were cut from different parts of the samples to form the half gram measured with coincidence.

Table 10 Data of the glass samples. Gd concentration was measured by the Compton suppressed PGAA spectrometer

Sample number	0	1	2	4
Sample mass [g]	0,529	0,536	0,449	0,48
Measuring time [minutes]	1052	1179	1220	325
Gd concentration [ppm]	0,87	1,4	11,9	21,9
Uncertainty of Gd conc.[ppm]	0,14	0,1	1,5	1,5

Table 10 presents the data of the four glass samples: the number of the sample for reference, the mass of the borated glass sample (used for the coincidence measurement), the measuring time (equal to the irradiation time), and the Compton suppressed measurement results; Gd concentration with its statistical uncertainty calculated with the method described in chapter 4.4.3. As can be seen in the table, very long measurement times were required to obtain acceptable peak statistics for the Gd peaks.

Sample “0” was taken just before the inactive gadolinium tracer was put into the furnace, so this measurement represents the natural gadolinium concentration of the glass.

5.9.2. Coincidence measurement results

The coincidence measurements were performed with the standard setup as described in chapter 5.1.

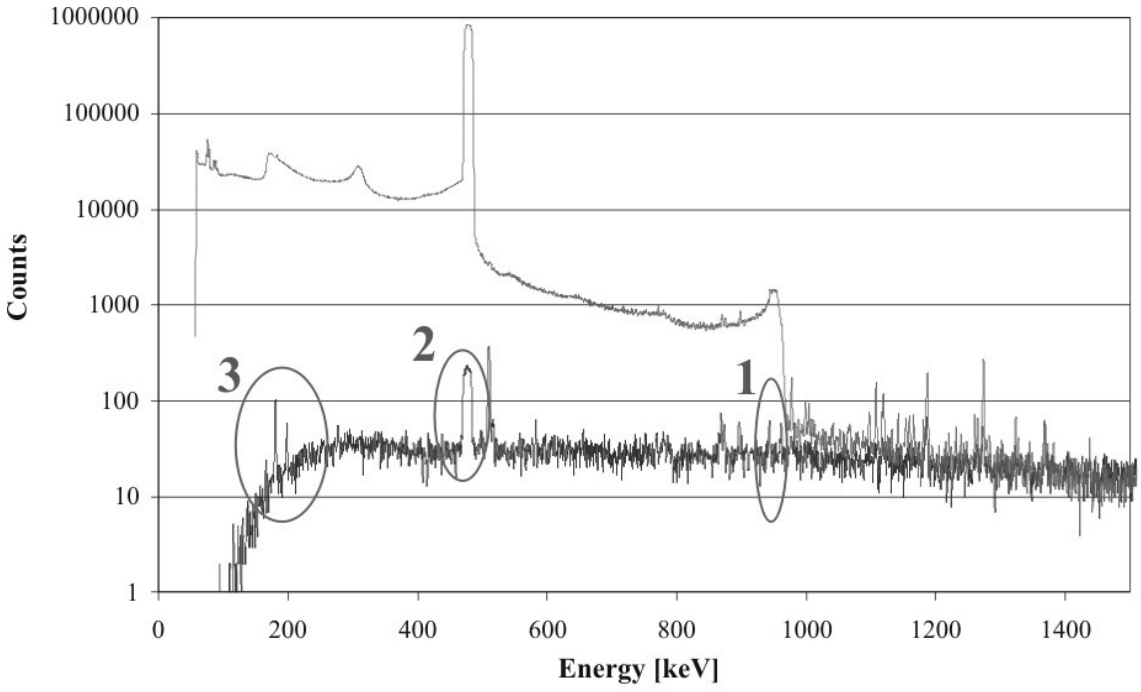

Figure 49 gadolinium traced borosilicate glass spectra of sample S1 in regional coincidence E>980keV (thick line) and Compton-suppressed (thin line) measurements

Figure 49 shows the spectra of the sample S1 measured with Compton suppressed spectrometer (same as Figure 27) and the coincidence method. The coincidence spectrum was created by defining a coincidence relation with every event having energy higher than 980 keV (above the boron double peak). Although the two spectra seem to be normalized for the energies above 1 MeV, they were not.

When jumping to a conclusion based on the spectra on Figure 49 about the performances of the two methods, one must take into consideration that almost all measurement parameters were different:

- In the Compton suppressed case, about 50 grams of sample was measured for ~5.5-20 hours, while with the coincidence method, 0.5 grams for 4 hours

- As the Compton suppressed measurement was carried out prior to, while the coincidence measurement after the construction of the cold neutron source, the latter had a neutron flux 20 times higher.

The spectra shapes obtained with the methods can be compared quantitatively (Figure 49):

1. The boron double peak and its Compton plateau were completely eliminated from the coincidence spectra.
2. The 478 keV boron peak and its Compton plateau were suppressed by a factor of 1000.
3. The evaluation of the 182, 199 keV gadolinium peaks became possible.

Because of this, the evaluation of the gadolinium peaks became as simple as a routine PGAA evaluation.

Figure 50 shows the calibration curve of the 182 keV gadolinium peak for the coincidence measurement obtained from the measurements of the four samples.

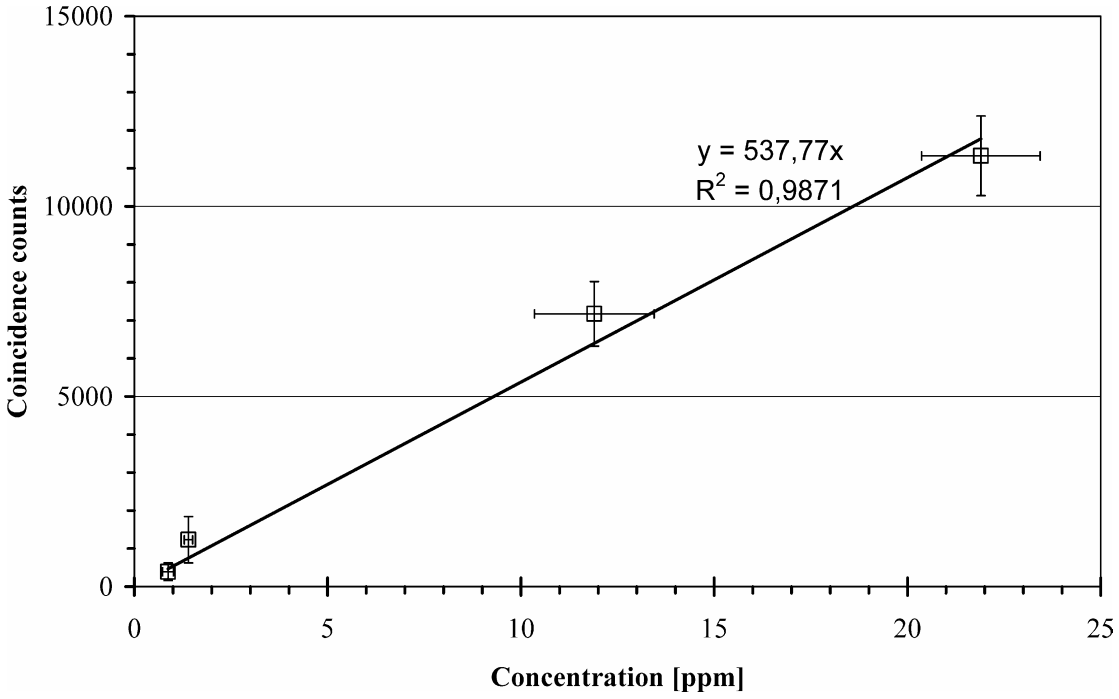

Figure 50 Calibration curve for the 182 keV gadolinium peak.

The peak areas were normalized for each sample to 1 gram sample mass and 1000 minutes of measurement time. The flux correction was made based on the integral of the boron peak in the singles mode spectra. The calibration curve contains the normalized peak areas for the 182 keV gadolinium peak as the function of the gadolinium concentration calculated from the Compton suppressed measurement (see Table 10). Each point has the uncertainty marked in both directions. The graph also shows the fitted linear function which was forced to cross the origin. The R^2 value of the fit is also marked on the graph. Although the figure above contains only four points, considering the large concentration (around 5%) of boron in the samples, the resulting calibration curve shows the strength of the method.

6. Summary

PGAA studies were started at the Budapest research reactor in 1995. The coincidence studies which I have participated in were started in 1998. For preliminary studies we used the target chamber of the existing Compton suppressed spectrometer. The experience with this target chamber helped the construction of a second facility [Belgya 02], called Neutron Induced Prompt Gamma Spectroscopy (NIPS). It was finished in 2001, parallel with the installation of the cold source and the reconstruction of the neutron guides. With its three detector positions, the NIPS facility was designed for PGAA, nuclear structure or even fission product studies using coincidence detection. I studied the usefulness of γ–γ coincidences in PGAA measurements using the new NIPS facility. I began my work with the simplest γ–γ coincidence measurements:

First I used two HPGe detectors for γ–γ coincidence experiment with a Co-60 source [Ember 02a]. I analyzed peak to peak coincidences in the list mode data. I found that the setup with peak to peak coincidence simplifies the spectrum substantially by showing the only coincident peak. By putting energy gates on both Co-60 peaks, I found an FWHM of about 13 ns for the projected time peak.

In the second measurement, I measured a chlorine sample in beam. This measurement yielded a total projected time resolution of 30 ns due to the time walk of the detectors, while the peak to peak time resolution was similar to the Co-60 case. Some coincidence cascades were also studied to confirm that I observe only coincidence peaks in the projections.

My final goal was to study the usefulness of coincidence method for elemental analysis. First I used a sample of known composition. It was a solution of cobalt chloride and boric acid. The hydrogen and boron were chosen to simulate the matrix effect: The most intense peaks of chlorine and cobalt are situated on the high Compton background of these two elements, also the most intense cobalt peak at 229 keV had a difficult spectral interference with the back-scattering of hydrogen. I found that the coincidence method could easily remove the hydrogen peak and its continuum, and also substantially reduce the number of boron events.

I also compared the γ–γ coincidence method with the singles mode and the Compton suppressed spectroscopy. I found that the γ–γ coincidence method can only be a competitive

alternative if I use the so-called regional coincidence method: instead of defining coincidence between photo peaks (called peak to peak coincidence), I define the coincidence also with a part of the Compton background. I found that this new approach is not so selective, but increases the peak efficiency substantially. The optimal peak to background ratio can be obtained by changing the amount of Compton background in the gate setting. For comparability, I measured the same sample with the same detector for the same length of time under all three setups. In the case of the γ–γ coincidence experimental setup, the gate range was set on all the energies higher than the hydrogen peak. Through comparison, I obtained the following results [Ember 02]:

1. Compton suppression reduces the hydrogen single-escape peak to full-energy peak ratio by a factor of 10, and reduces the double-escape peak to unidentifiable, while the coincidence completely eliminates the hydrogen peak, its Compton edge, and both of its escape peaks.
2. Compared to the single measurement, the continuous Compton background is lowered by a factor of ~100 at γ-ray energies between 1 and 2 MeV in the Compton-suppressed case. However, the boron peak and its Compton background still dominate the low-energy part of the spectrum. Peaks below the boron peak can hardly be seen on this background. The Compton background due to boron is reduced only by a factor of 20-40, showing that the Compton suppression is very energy dependent. Both of the Compton continuum reductions involve the larger detector to sample distance (reduction factor of ~9) and the Compton suppression as well. In the coincidence case the boron peak and its Compton continuum are also reduced substantially, making the low-energy γ rays much more visible.
3. Compton suppression gives a 1.5-2 times better peak-to-background ratio than the ungated singles, while the coincidence method gives a 25-40 times better value at low energies. Under the present secondary detector and gating conditions, the signal/noise ratio for the highest energy (1164 keV) is best with the Compton suppression.

I found that comparing the Compton suppressed method with the coincidence is not simple. There is no obvious answer to the question on which of the methods is better. For a given sample, for a given peak of interest, a given coincidence setup of the same detector can produce better or worse peak to total ratio, but can not be better in all cases. It is also possible to define different optimal gate for every peak in the spectra. If the same gate is defined for

the same peak in a series of measurements the comparability is not lost this way, and the relative method could still be applied for the calculation of the concentrations.

To prove that the coincidence method is capable of elemental analysis, I performed a series of measurements with solutions having different cobalt-chloride concentration. Calibration curves were determined for the two most intense peaks of cobalt at 229 keV and 277 keV, and for a chlorine doublet at 1164 keV for comparison. I found that the count rate increases linearly with the concentration, therefore the method can be used for analytical work.

In order to make use of the new regional coincidence method, a series of gadolinium traced borosilicate glass samples – used in a previous industrial measurement – were re-measured. My goal was to see if the γ-γ coincidence method can eliminate the matrix effect even in a difficult case. The samples contained about 5% of boron, and every gadolinium peak had some spectral interference disturbing the evaluation. The 182 and 199 keV peaks were situated on the Compton background of the boron peak, the 944 keV peak was interfering with the 2*478 keV boron sum peak, and the 1184 and 1186 keV peaks were interfering with each other. The coincidence spectrum was created by defining coincidence relation with every event having energy higher than 2*478 keV. I observed the following facts [Ember 01, Ember 02b]:

1. The boron double peak and its Compton plateau were completely eliminated from the coincidence spectra.
2. The 478 keV Boron peak, and its Compton plateau were suppressed by a factor of 1000.
3. The evaluation of the 182, 199 keV peaks became possible.

Since the regional coincidence method is more complicated than the traditional PGAA method, it should be used only for very difficult cases.

7. Thesis

This work contains the following new results:

I. I adopted the γ-γ coincidence method for PGAA with two HPGe detectors for the first time in the world:

a. Based on experiments I found an optimal geometry for the γ-γ coincidence method: when the detectors are at the closest to the sample (covering maximum solid angle). And the mass of the sample is chosen to cause no substantial pile-up (~10 000 count/second was ideal in the case of the detectors used). The NIPS facility of the institute was designed according to these experiments.

b. After testing many electronic setups I choose and set up one that provides reproducible measurements, and detects only a small amount of non coincidence events.

c. I improved the software for the evaluation of the off-line recorded measurement results:

   i. to define gates

   ii. and to create gated spectra

II. I worked out the concept of the regional coincidence:

In the case of peak to peak coincidence, coincidence with a photo peak is required. According to the peak to total ratio in the function of energy, at high energy this method rejects the majority of the events. In the case of regional coincidence, a part of the Compton background is also accepted. This way more events are got (so the peak statistics is better), but also more random coincidence events are counted in, increasing the background bellow the peak. I obtained the optimal setting (the part of the Compton background accepted) experimentally for every case investigated. And I found that the regional coincidence method substantially increased the efficiency of the γ-γ coincidence method in many cases.

III. **I proved that the γ-γ coincidence method is capable of decreasing the matrix effect, and simplify the PGAA spectra:**

a. I proved with experiments that, by choosing the (regional) coincidence gates correctly the PGAA spectra can be simplified remarkably: background peaks and other irrelevant or disturbing peaks can be completely eliminated. As the processing is off-line; a distinct optimal gate can be defined even on every peak of the

spectrum. This solution does not corrupt the comparability of the elements in a series of measurements.

b. I demonstrated with test samples that peaks of the single-line sources (like Boron and Hydrogen) can be be decreased by orders of magnitude or even eliminated completely with γ-γ coincidence method from the spectra even in cases of high concentration. It makes the evaluation of lower intensity peaks (that would otherwise be lost in the statistical fluctuation of the background) possible:
    i. The Boron double peak at 2*478 keV and its Compton background can be eliminated completely. The Boron peak at 2*478 keV and its Compton background can be decreased by orders of magnitude.
    ii. The Hydrogen peak at 2223 keV and its Compton background can be eliminated completely.
    iii. The back scatter peaks caused by the geometry of the setup can be eliminated completely.

    Thus I proved that, the γ-γ coincidence method is capable of decreasing the matrix effect, and simplify the PGAA spectra.

c. An industrial inactive tracing method of glass furnaces was developed at our institute recently. Gadolinium tracer is used for measurements of glass samples containing Boron. In this case, matrix effect is a real problem. With the usage of the coincidence method I succeeded to evaluate such Gadolinium peaks, that were neglected in the case of Compton suppression technique, because of the spectral interferences. Thus I demonstrated the usefulness of the method in the case of an industrial application.

IV. I proved that the γ-γ coincidence method can be used for analytical work and its sensitivity can compete with the traditional methods in certain cases :

a. I made calibration curves by measuring known concentration sample series. I found that the peak counts are linear with the concentration even in the case of strong matrix effect. The parameters of this linear function are depending on the gates set. I concluded that the γ-γ coincidence method can be used for analytical work. And I found that (just like in the case of Compton suppression technique) the detection limit differs for each element, and also depends on the matrix.

b. I compared the γ-γ coincidence method with the Compton suppression technique, and the simple single detector measurement in the cases of different kinds of

samples. I found that, in the low energy range (E<1MeV) it is possible to find a gate setting for most peaks in every sample when the usage of the regional coincidence gives comparable or even better peak-background ratio. With the usage of higher efficiency HPGE detectors, this energy range can be broadened.

7.1. Publications

List of own publications and presentations, connected to the subject of the Ph.D. thesis:

[1] Ember, P.P., Belgya, T., Molnár, G.L., **2002.** Improvement of the capabilities of PGAA by coincidence techniques, Applied Radiation and Isotopes **56**, 535-541.

[2] Ember, P.P., Révay, Zs., Belgya, T., Molnár, G.L., Varga, Zs., **2001.** Inaktív nyomjelzés prompt gamma aktivációs módszerrel, Magyar Kémiai Folyóirat **107**, 438-443.

[3] Ember, P.P., Belgya, T., Molnár, G.L., **2002.** Coincidence Measurement setup for PGAA and nuclear structure studies, Applied Radiation and Isotopes, **57**, 573-577. (Thesis-points: I, II)

[4] Ember, P.P., Belgya, T., Weil J.L., Molnár, G.L., **2004.** A practical test of a γ-γ coincidence measurement setup for PGAA, Nuclear Instruments and methods B. 213, 406-409

[5] Belgya, T., Révay, Zs.,. Ember, P.P, Weil, J.L., Molnár, G.L., The cold neutron PGAA-NIPS facility at the Budapest Research Reactor, **2003**. 262-271. Capture Gamma-Ray Spectroscopy and Related Topics, World Scientific Pub Co Inc, Singapore.

[6] Révay, Zs., Belgya, T., Ember, P.P., Molnár, G.L., **2001.** Recent developments in HYPERMET-PC, Journal of Radioanalytical and Nuclear Chemistry, **248**, 401-405.

[7] Ember, P.P., Belgya, T., Molnár, G.L., **2000.** Coincidence method for determination of peak to total ratios of HPGe gamma-ray detectors, Budapest Neutron Centre Progress Report 1998- 1999, 114.

[8] Ember, P.P., Belgya, T., Molnár, G.L., **2000.** Improvement of detection limit and element selectivity by coincidence techniques in PGAA; in Budapest Neutron Centre Progress Report 1998- 1999, 115.

Presentations:

[9] Ember, P.P., Belgya, T., Molnár, G.L., Csúcs/összes viszony vizsgálata a csúcs energiájának függvényében, Őszi Radiokémiai napok, Kecskemét, **1999**

[10] Ember, P.P., Belgya, T., Molnár, G.L., A PGAA elemi érzékenységének növelése koincidencia technikával, Központi Kémia Schay Géza emlékülés, **2000**

[11] Ember, P.P., Belgya, T., Molnár, G.L., A PGAA elemi érzékenységének növelése koincidencia technikával; Őszi Radiokémiai napok, Hévíz, **2000**

[12] Ember, P.P., Belgya, T., Weil, J.L., Molnár, G.L., A practical test of a γ-γ coincidence measurement setup for PGAA, Poster on IRRMA-V conference in Bologna **2002**

[13] Belgya, T., Révay, Zs.,. Ember, P.P, Weil, J.L., Molnár, G.L., The cold neutron PGAA NIPS facility at the Budapest Research Reactor; Eleventh International Symposium on Capture Gamma-Ray Spectroscopy and Related Topics, Pruhonice near Prague, Czech Republic September 2 - 6, **2002**

8. Possible usage of the results

An advantage of the A γ-γ coincidence method is that it does not require special detector system like the Compton suppression unit. Although it requires preprocessing of the data, the final spectra is simplified till the level of automatic evaluation. The method can be used for automating routine measurements.

The method can also be used for portable PGAA measurements with greater efficiency detectors.

Because of the variability of the coincidence gates, an absolute calibration method would be very difficult, so a standard based relative method should be applied for the calculation of the concentrations.

9. Acknowledgement

First of all, I have to thank for my supervisor Tamás Belgya, who helped me in every aspect from the beginning. Csaba Sükösd was my university consultant, who even covered me, when I forgot to do some paperwork. And sometimes I did.

Also there are my colleagues at the department of nuclear physics, who also helped me with some ideas and other support.

As the leader of the department Gabor Molnár oversee the project, and also helped with the papers. Zsolt Révai helped with the Compton suppressed spectrometer. Prof. Jesse Weil helped my technical English.

Gwen was the lector of my English.

I must also thank my home defense opponents for the new point of view.

10. References

[Ama 34] E. Amaldi, O'd. Agostino, B. Pontecorvo, E. Segré, Recerca Sc. 2 467 **1934**; D. E. Lea, Nature **133** 24

[Beckurts 64] K.H. Beckurts, K.Wirtz: Neutron physics, Springer Verlag, **1964**

[Belgya 96] Belgya, T., Révay, Zs., Fazekas, B., Héjja, I., Dabolczi, L., Molnár, G.L., Kis, Z., Östör, J., Kaszás, Gy., **1996**. The New Budapest Capture Gamma-ray facility, Proceedings of the Ninth International Symposium on Capture Gamma-Ray Spectroscopy and Related Topics, Vol. 2, Budapest, Hungary, 826.-837.

[Belgya 02] Belgya, T., Révay, Zs.,. Ember, P.P, Weil, J.L., Molnár, G.L., The cold neutron PGAA- NIPS facility at the Budapest Research Reactor, **2003**. Capture Gamma-Ray Spectroscopy and Related Topics, World Scientific Pub Co Inc, Singapore, 262-271.

[BNC 00] Budapest Neutron Centre Progress Report 1998-1999, Budapest, **2000**

[ehman 91] Ehmann, W. D., Vance, D. E., **1991** Radiochemistry and nuclear methods of analysis. Wiley-interscience, New York

[Ember 01] Ember, P.P., Révay Zs., Belgya, T., Molnár, G.L., Varga Zs., **2001**. Inaktív nyomjelzés prompt gamma aktivációs módszerrel, Magyar Kémiai Folyóirat **107** 438-443.

[Ember 02] Ember, P.P., Belgya, T., Molnár, G.L., **2002**. Improvement of the capabilities of PGAA by coincidence techniques, Applied Radiation and Isotopes, **56**, 535-541.

[Ember 02a] Ember, P.P., Belgya, T., Molnár, G.L., **2002**. Coincidence Measurement setup for PGAA and nuclear structure studies, Applied Radiation and Isotopes, **57**, 573-577.

[Ember 02b] Ember, P.P., Belgya, T., Weil J. L., Molnár, G.L., **2002.** A practical test of a γ-γ coincidence measurement setup for PGAA, Nuclear Instruments and methods B. In press

[Fazekas 97] Fazekas, B., Molnár, G.L., Belgya, T., Dabolczi, L., Simonits, A., **1997**. Introducing HYPERMET-PC for automatic analysis of complex gamma-ray spectra, Journal of Radioanalytical and Nuclear Chemistry. **215**, No.2, 271-277.

[Fazekas 98] Fazekas, B., Östör, J., Kiss, Z., Simonits, a., Molnár, G.L., **1998**, Quality assurance features of "HYPERMET-PC", Journal of Radioanalytical and Nuclear Chemistry. **233**, 101-103.

[Fermi 47] Fermi et al 1947 Science **105** 27

[Firestone 96] Firestone, R.B., **1996**. Table of Isotopes 8th edition, John Wiley & Sons, Inc., New York

[Földiák 72] Földiák, G., **1972**. Az izotópok ipari alkalmazása, Műszaki könyvkiadó, Budapest, 205-206.

[Gardner 00] Gardner, R.P., Mayo, C.W., El-Sayyed, E.S., Metwally, W.A., Zheng, Y., Poezart, M., **2000**. A feasibility study of a coincidence counting approach for PGNAA applications, Applied Radiation and Isotopes, **53**, 515-526.

[Héjja 97]Héjja, I., Belgya, T., Molnár, G.L., 1997. Multiparameter data acquistion and analysis system for capture gamma-ray studies, **1997.** Proceedings of the Ninth International Symposium on Capture Gamma-Ray Spectroscopy and Related Topics, Vol. 2, Budapest, Hungary 933.-934.

[hen 73] R. Henkelmann, H.-J. Born, **1973** J. Radioanal Chem. **16** 473

[Jakubek 98] Jakubek, J., Nuiten,P., Pluhař, J., Popíšil, S., Šinor, M., Štekl, I., Timorácký, S., Vobecký, M., **1998**. Coindence gamma-gamma spectroscopy system for

instrumental neutron activation analysis. Nuclear Instruments and Methods A, **414**, 261-264.

[Kasztovszky 00] Kasztovszky, Zs., Révay, Zs., Belgya, T., Molnár, G.L., **2000.** Nondestructive analysis of metals by PGAA at the Budapest Research Reactor, Journal of Radioanalytical and Nuclear Chemistry, **244,** 379-382.

[Koeberl 00] Koeberl, Ch., Huber, H., **2000**. Optimalization of the multiparameter γ-γ coincidence spectrometry for the determination of iridium geological materials. Journal of Radioanalytical and Nuclear Chemistry, **244**, 655-660.

[Knoll 00] Knoll, G.F., **2000**. Radiation Detection and Measurement, 3rd Edition John Wiley & Sons, Inc., New York

[Lindstrom 93] Lindstrom, R.M., Zeisler, R., Vincent, D.H., Greenberg, R.R., Stone, C.A., Mackey, E. A., Anderson, D. L., Clark, D. D., **1993** Neutron-capture prompt gamma-ray activation-analysis at the NIST cold neutron research facility, Journal of Radioanalytical and Nuclear Chemistry, **167**, 121-126.

[Lindstrom 93-2] R. M. Lindstrom, E. A. Mackey, R. L. Paul: Int. Conf. **1993**. Anal. Methods in the life Sciences. Prague Sept

[Lindstrom 94] Lindstrom, R. M., Paul, R. L., Vincent, D. H., Greenberg, R. R., **1994** Measuring hydrogen by cold-neutron prompt gamma activation-analysis, Journal of Radioanalytical and Nuclear Chemistry, **180**, 271-275.

[Meyer 87] Meyer, G. J., **1987**. Multiparameter coincidence spectrometry applied to the instrumental activation analysis of rocks and minerals. Journal of Radioanalytical and Nuclear Chemistry, **114**, 223-230.

[Meyer 93] Meyer, G., Piccot, S., Rocchia R., Toutain J.P., **1993**. Simultaneous determination of Ir and Se In K-T boundary clays and volcanic sublimates. Journal of Radioanalytical and Nuclear Chemistry, **168**, 125-131.

[Molnár 97] Molnár, G., Belgya, T., Dabolczi, L., Fazekas, B., Révay, Zs., Veres, Á., Bikit, I., Kiss, Z., Östör, J., **1997.** The new prompt gamma-activation analysis facility at Budapest, Journal of Radioanalytical and Nuclear Chemistry, **215** 111-115.

[Molnár 98] Molnár, G.L., Lindstrom, R.M., **1998**. Nuclear methods in mineralogy and Geology, Plenum Press, New York, London, (Chapter 3.) 145-164.

[Molnar 00] Molnár, G. L., Révay, Zs., Belgya, T., Firestone, R.B., **2000**. The new prompt gamma-ray catalog for PGAA, Applied radiation and Isotopes, **53**, 527-533.

[Molnár 02] Molnár, G. L., Révay, Zs., Belgya, T., **2002**. Wide-energy range efficiency calibration method for Ge-detectors, Nuclear Instruments and Methods A. **489** 140-159.

[Paul 94] R. L. Paul, R. M. Lindstrom: **1994** Rev. Prog. Quantitative Nondestructive Evaluation 13 Premium Press, New York,. 1619.

[Phillips 76] Phillips, G. W., Marlow, K. W., **1976**. Program HYPERMET for automatic analysis of gamma-ray spectra from germanium detectors, Nuclear Instruments and Methods **137** 525-536.

[Révay 98] Zs. Révay, Zs. Kasztovszky, T. Belgya B. Fazekas, J. Östör, G. L. Molnár: **1998** Determination of nuclear data of elements for PGAA, in J. Gadó, L. Rosta, I. Vidovszky *Eds.* : Budapest Neutron Centre Progress Report 1994- 97, Budapest, 93.

[Révay 01] Révay, Zs., Molnár, G. L., Belgya, T., Kasztovszky, Zs., Firestone, R. B., **2001**. A new gamma-ray spectrum catalog and library for PGAA, Journal of Radioanalytical and nuclear Chemistry **248**, 395-399

[Révay 01a] Révay, Zs., Belgya, T., Ember, P.P., Molnár, G.L., **2001.** Recent developments in HYPERMET-PC, Journal of Radioanalytical and Nuclear Chemistry, **248**, 401-405.

[Révay 02] Zs.Révay ,T.Belgya,Zs.Kasztovszky,J.L.Weil,G.L.Molnár COLD NEUTRON PGAA FACILITY AT BUDAPEST Talk presented at the 5 th Int.Topical Meeting on Industrial Radiation and Radioisotope Measurement applications IRRMA-V Bologna, Italy, 9-14 June **2002**

[Rosta 02] Rosta, L., Cser, L., Révay Zs., **2002**. Gain factors with the new supermirror guide system at the Budapest Neutron Centre, Applied Physics A, **75**, 1-3.

[TOF 99] Firestone, R.B., **1999.** Table of Isotopes John Wiley & Sons, Inc., New York

[Yonezawa 93] Yonezawa, C., **1993.** Prompt gamma-ray analysis of elements using cold and thermal reactor guided neutron beams, Analytical Sciences, **9**, 185-193.

[wapstra 79] Wapstra, A.H., **1979.** Alpha-, Beta- and Gamma-ray Spectroscopy, 5th printing, North Holland Publishing Company: Amsterdam New York Oxford, Volume I, Chapter VIII/C, 539-555.

Appendix A: Parameters of the PGAA facility

Table 11 shows the specifications of the Compton suppressed spectrometer facility. Table 12 shows its Detection limit for different elements [Révay 02].

Table 11 Main specifications of the Compton suppressed spectrometer

Target position:	1,5 m from the end of the guide NG-1
Beam cross section	Max. 2cm x 2 cm
Thermal-equivalent flux at target	~ $5*10^7$ $cm^{-2}s^{-1}$
Vacuum in target chamber (optional)	~1 mbar
Target chamber Al-window thickness	0.5 mm
Form of target at room temperature	Solid, powder, liquid, or gas in pressure container
Target packing	Sealed FEP Teflon bag or Teflon vial
Activity of trget after irradiation	Negligible
Largest target dimensions	5 cm x 5 cm x 5 cm
Distance from target to detector window	235 mm
γ-ray detector	n-type coax. HPGe with BGO shield
HPGe window	Al, 0.5 mm
Relative HPGe efficiency	25% at 1332 keV (^{60}Co)
HPGe FWHM	1.8 keV at 1332 keV (^{60}Co)
Compton suppression enhancement	~5 at 1332 keV and ~40 at 7000 keV
Room background	0.5 cps
beam background	8 cps with both upper and lower beam open and 4 cps with only one of them

Table 12 detection limits of different elements

Detection limits [μg/g sample]	**Elements**
<0,1	B, C, Sm, Gd, Eu
0,1-10	Cl, Sc, Ti, V, Co, Rh, In, Xe, Hf, Re, Hg, Nd, Dy, Er
10-100	H, Na, K, Cr, Mn, Ni, Cu, As, Se, Br, Sr, Mo, Ag, Cs, Ta, Os, Pt, Au, Ho, Tm, Yb, Lu, U
100-1000	Li, Be, Mg, Al, Si, P, S, Ca, Fe, Zn, Ga, Ge, Rb, Y, Zr, Nb, Ru, Pd, Sb, Te, I, Ba, La, W, Ir, Tl, Ce, Pr, Th

Efficiency calibration has been made for the PGAA spectrometer from 50 keV to 11 MeV using radioactive sources and (n,γ) reactions. Its accuracy is better than 1% from 50 keV to 8 MeV [Molnár 02]. The obtained efficiency function can be seen in Figure 51.

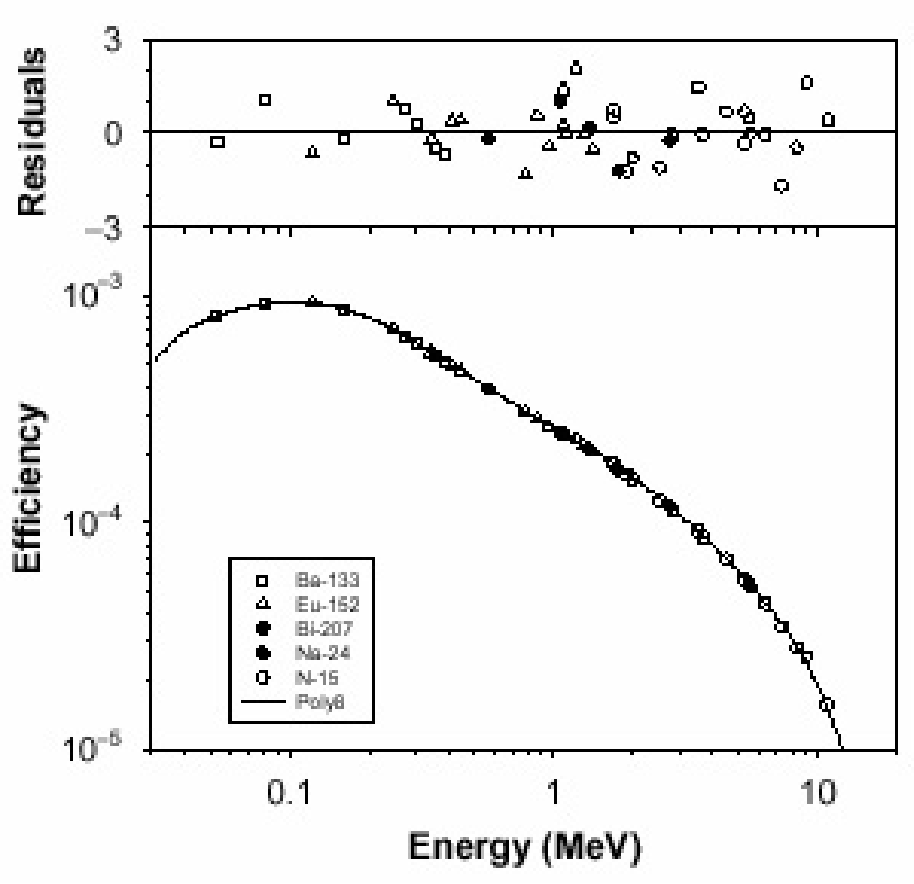

Figure 51 Relative full energy peak efficiency (lower curve), and the corresponding normalised residuals (upper curve) for the Compton suppressed spectrometer

Appendix B: Parameters of the NIPS facility

Table 13 shows the specifications of the NIPS facility [Révay 02].

Table 13 Main specifications of the NIPS facility

Target position:	2,6 m from the end of the guide NG-1
Beam cross section	Max. 2cm x 2 cm
Thermal-equivalent flux at target	~ $3*10^7$ $cm^{-2}s^{-1}$
Vacuum in target chamber (optional)	~1 mbar
Target chamber Al-window thickness	0.5 mm
Form of target at room temperature	Solid, powder, liquid, or gas in pressure container
Target packing	Sealed FEP Teflon bag or Teflon vial
Activity of target after irradiation	Negligible
Largest target dimensions	1.5 cm diameter, 3.5 cm length
Distance from target to detector window	Minimum 25 mm
Possible γ-ray detector 1 HPGe window Relative HPGe efficiency HPGe FWHM	n-type coax. HPGe Carbon 15% at 1332 keV (^{60}Co) 1.8 keV at 1332 keV (^{60}Co)
Possible γ-ray detector 2 HPGe window Relative HPGe efficiency HPGe FWHM	n-type coax. HPGe Be, 0.5 mm 30% at 1332 keV (^{60}Co) 1.9 keV at 1332 keV (^{60}Co)
Possible γ-ray detector 3 HPGe window HPGe FWHM	Planár HPGe Be, 0.5 mm 0.6 keV at 1332 keV (^{60}Co)

Appendix C: Parameters of the isotopes

This chapter contains the most intense gamma lines for the isotopes mentioned in this work, obtained from [TOF 99]. **Eg** marks the gamma energy in keV, **RI** marks the relative intensity of the peak. In the case Gd only the two most important isotopes of natural Gd are shown.

Gammas for :**1H**(n,γ) 2H

Eg	RI
2223.245	100

Gammas for :**10B**(n,α) 7Li

Eg	RI
477.595	

Gammas for :**16O**(n, γ) 17O

Eg	RI
870.71	100
1087.93	82
2184.48	82
3272.26	18

Gammas for :**35Cl**(n, γ) 36Cl

Eg	RI
1164.867	100.0
517.07340	89
6110.853	74.9
1951.142	72.9
788.4281	59.3
1959.348	46.3
7413.979	39.4
786.3021	37.6
7790.343	34.0
6619.627	31.8
2863.823	21.0
5715.253	20.27
6627.832	17.4
4979.771	13.4
3061.869	12.87
1601.074	12.8
8578.588	11.2
6977.847	8.48
1162.741	8.1
1131.250	6.89
5517.223	6.17
2676.338	6.1
2845.503	4.62
1327.404	4.48

Gammas for :**59CO**(n, , γ) 60Co

Eg	RI
229.72	15.18
277.08	13.96
555.972	11.97
6877.40	8.42
6706.22	7.54
5660.51	7.14
447.68	7.00
5976.13	6.90
6486.61	6.25
1515.769	5.55
1830.793	5.50
785.730	5.33
497.277	4.46
7214.79	3.70
7491.99	2.88
6985.61	2.76
254.23	2.75
5181.74	2.67
158.46	2.438
391.222	2.290
5742.78	2.17
945.329	2.04
5925.98	1.81
717.420	1.792

Gammas for:**155Gd**(n, γ) 156Gd

Eg	RI for 1000 γ rays
199.21900	316E+1
88.970	209E+1
1159.031	68E+1
1065.1781	564
1230.6857	556
1154.1467	50E+1
1187.1631	454
1040.470	297
1242.481	285
1277.482	255
296.532	253
1180.3119	249
969.865	248
1067.2325	232
1153.478	232
987.948	205
1222.427	194
1169.087	180
959.820	173
1250.655	157
1682.174	157
1449.897	146
1174.188	144

Gammas for:**157Gd** (n, γ) 158Gd

Eg	RI for 1000 γ rays
181.930	1.95E3
79.5104	1037
944.09	910
962.06	580
1107.63	480
1185.99	455
977.06	411
1187.13	401
897.59	348
1119.16	332
897.59	312
6750.0	294
780.14	266
1183.97	263
1097.01	191
1323.39	181
1263.54	175
998.36	158
1141.44	154
5903.2	150
1116.48	121
277.544	120
1004.00	118